

# Plant Hydraulic Transport Controls Transpiration Sensitivity to Soil Water Stress

Brandon P. Sloan<sup>1,2</sup>, Sally E. Thompson<sup>3</sup>, and Xue Feng<sup>1,2</sup>

<sup>1</sup>Department of Civil Environmental and Geo-Engineering, University of Minnesota - Twin Cities, Minneapolis, MN 55455

<sup>2</sup>Saint Anthony Falls Laboratory, University of Minnesota - Twin Cities, Minneapolis, MN 55455

<sup>3</sup>Department of Civil, Environmental and Mining Engineering, University of Western Australia, Perth, Australia

**Correspondence:** Brandon Sloan (sloan091@umn.edu), Xue Feng (feng@umn.edu)

**Abstract.** Plant transpiration downregulation in the presence of soil water stress is a critical mechanism for predicting global water, carbon, and energy cycles. Currently, many terrestrial biosphere models (TBMs) represent this mechanism with an empirical correction function ( $\beta$ ) of soil moisture—a convenient approach that can produce large prediction uncertainties. To reduce this uncertainty, TBMs have increasingly incorporated physically-based Plant Hydraulic Models (PHMs). However, PHMs introduce additional parameter uncertainty and computational demands. Therefore, understanding why and when PHM and  $\beta$  predictions diverge would usefully inform model selection within TBMs. Here, we use a minimalist PHM to demonstrate that coupling the effects of soil water stress and atmospheric moisture demand leads to a spectrum of transpiration response controlled by soil-plant hydraulic transport (conductance). Within this transport-limitation spectrum,  $\beta$  emerges as an end-member scenario of PHMs with infinite conductance, completely decoupling the effects of soil water stress and atmospheric moisture demand on transpiration. As a result, PHM and  $\beta$  transpiration predictions diverge most for soil-plant systems with low hydraulic conductance (transport-limited) that experience high variation in atmospheric moisture demand and have moderate soil moisture supply to plants. We test these minimalist model results by land surface modeling an Ameriflux site. At this transport-limited site, a PHM downregulation scheme outperforms the  $\beta$  scheme due to its sensitivity to variations in atmospheric moisture demand. Based on this observation, we develop a new ‘dynamic  $\beta$ ’ that varies with atmospheric moisture demand—an approach that overcomes existing biases within  $\beta$  schemes and has potential to simplify existing PHM parameterization and implementation.

## 1 Introduction

Plants control their transpiration ( $T$ ) and  $\text{CO}_2$  assimilation by adjusting leaf stomatal apertures in response to environmental variations (Katul et al., 2012; Fatichi et al., 2016). In doing so, they mediate the global water, carbon, and energy cycles. The performance of most terrestrial biosphere models (TBMs) relies on accurately representing leaf stomatal responses in terms of stomatal conductance ( $g_s$ ). Extensive research has established the relationships between  $g_s$  and atmospheric conditions like photosynthetically active radiation, humidity,  $\text{CO}_2$  concentration, and air/leaf temperature under well-watered conditions, though the specific forms of these relationships vary (Damour et al., 2010; Buckley et al., 2014; Buckley, 2017). However, representing the dynamics of  $g_s$  in response to soil water stress remains problematic.

25 Many TBMs represent declining  $g_s$  and, in turn, transpiration reduction (i.e., downregulation) in response to soil water stress with an empirical function of soil water availability. This method, known as  $\beta$  (Powell et al., 2013; Verhoef and Egea, 2014; Trugman et al., 2018; Paschalis et al., 2020), reduces  $g_s$  from its peak value under well-watered conditions ( $g_{s,ww}$ ), i.e.,  $g_s = \beta \cdot g_{s,ww}$ ,  $0 \leq \beta \leq 1$ . (We use the term ' $\beta$ ' in this paper to refer to the downregulation model itself, and the terms ' $\beta$  function' or ' $\beta$  factor' to refer to the empirical function and its values, respectively.) The term 'well-watered' refers to moist  
30 soil conditions where stomatal aperture is unaffected by soil water uptake, i.e., no soil water stress. Using a  $\beta$  function to reduce well-watered transpiration (or  $g_s$ ) originated, to the best of our knowledge, as a heuristic assumption in the crop transpiration model, SWATR (Feddes et al., 1978). Since then, it has gained widespread use within TBMs and hydrological models due to its parsimonious form.

However, mounting evidence indicates that using  $\beta$  in TBMs is a major source of uncertainty and bias in plant-mediated  
35 carbon and water flux predictions. Multiple studies have implicated the lack of a universal  $\beta$  formulation as a primary source of inter-model variability in carbon cycle predictions (Medlyn et al., 2016; Rogers et al., 2017; Trugman et al., 2018; Paschalis et al., 2020). For example, different  $\beta$  formulations among nine TBMs accounted for 40%-80% of inter-model variability in global gross primary productivity (GPP) predictions (on the order of 3-283% of current GPP) (Trugman et al., 2018). Aside from the uncertainty in functional form,  $\beta$  appears to fundamentally misrepresent the coupled effects of soil water stress and  
40 atmospheric moisture demand on stomatal closure. Recent work using model-data fusion at FLUXNET sites highlighted that  $\beta$  produces stomatal responses that are overly sensitive to soil water stress and unrealistically insensitive to atmospheric moisture demand (Liu et al., 2020). Furthermore, TBM validation experiments have found  $\beta$  schemes produce unrealistic GPP prediction during drought at Amazon rainforest sites (Powell et al., 2013; Restrepo-Coupe et al., 2017) and systematic overprediction of  
45 evapotranspiration duration, magnitude and intensity (Ukkola et al., 2017) at several Ameriflux sites. The apparent inadequacy of  $\beta$  has lead to the adoption of physically-based Plant Hydraulic Models (PHMs) in TBMs (Williams et al., 2001; Bonan et al., 2014; Xu et al., 2016; Kennedy et al., 2019; Eller et al., 2020; Sabot et al., 2020).

PHMs represent water transport, driven by a gradient of water potential energy, through the soil-plant-atmosphere continuum via flux-gradient relationships (based on Hagen-Poiseuille flow), which use measurable soil properties and plant traits as parameters (Mencuccini et al., 2019). The implementation of PHMs in several popular TBMs (e.g., CLM, JULES, etc.) has  
50 improved predictions in site-specific GPP and evapotranspiration (ET) predictions (Powell et al., 2013; Bonan et al., 2014; Eller et al., 2020; Sabot et al., 2020; Kennedy et al., 2019) as well as soil water dynamics (Kennedy et al., 2019) compared to  $\beta$ . PHMs also exhibit more realistic sensitivity to atmospheric moisture demand than  $\beta$  (Liu et al., 2020). However, these improvements from PHMs come at the cost of an increased number of plant hydraulic trait parameters and computational burden, which can reduce the reliability of the predictions (Prentice et al., 2015). Additionally, obtaining representative plant  
55 hydraulic trait values for a soil-plant system is difficult for two main reasons: i) traits vary widely across and within species (Anderegg, 2015) and exhibit plasticity through acclimation and adaptation (Franks et al., 2014), and ii) trait measurements are typically made at a single point (e.g., stem, branch, leaf), which may not be able to reliably scaled to represent whole-plant or ecosystem-level responses due to the effects of nonlinear trait variations along the soil-plant system (Couvreur et al., 2018). These difficulties result in uncertainty in the model predictions that may be further compounded at the ecosystem level (Fisher

et al., 2018; Feng, 2020). Consequently, modelers continue to rely on  $\beta$  as a parsimonious alternative to PHMs (Paschalis et al., 2020).

The relative strengths and weaknesses of  $\beta$  and PHMs suggest that informed model selection requires a better understanding of when the complexity of a PHM is justified over the simplicity of  $\beta$ . This paper informs such understanding by: i) analyzing the fundamental differences between PHMs and  $\beta$ , ii) defining the parameters controlling the differences (Sect. 3.2) and iii) demonstrating how PHMs outperform  $\beta$  for a real soil-plant system (Sect. 3.3). Then, leveraging our theoretical insights, we create a new ‘dynamic  $\beta$ ’ as a potential tool to correct the biases from the original  $\beta$  while reducing the parameter and computational demands of PHMs (Sect. 3.3). To accomplish these goals, we first analyze a minimalist PHM using a water supply-demand framework, then corroborate the results for a more widely-used, complex PHM, and, finally, perform a case study with a calibrated land surface model (LSM), which employs  $\beta$ , PHM, and ‘dynamic  $\beta$ ’ downregulation schemes.

## 2 Methods

### 2.1 Minimalist PHM

Our minimalist (Sect. 3.1-3.2) and complex PHM formulations (Sect. 3.3), illustrated in Fig. 1, rely on a supply-demand framework that conceptualizes transpiration as the joint outcome of soil water supply and atmospheric moisture demand (Gardner, 1960; Cowan, 1965; Sperry and Love, 2015; Kennedy et al., 2019). In this framework, ‘supply’ refers to the rate of water transport to the leaf mesophyll cells from the soil, into the roots, and through the xylem. ‘Demand’ refers to the rate of water vapor outflux through the stomata, driven by the transport capacity of the air surrounding the plant and regulated by the stomatal response to atmospheric conditions (Buckley, 2017) and leaf water status (Klein, 2014; Buckley, 2019). We assume steady-state transpiration fluxes (i.e., supply equals demand), which means we neglect the effects of plant capacitance (Bohrer et al., 2005) and also assume that the mean plant and atmospheric states equilibrate quickly over short timescales.

The minimalist PHM supply ( $T_s$  [mm day<sup>-1</sup>]; Eq. 1 and blue segment in Fig. 1a) is represented by a steady-state, integrated 1-D flux-gradient relationship, bounded by the root zone average soil water potential ( $\psi_s$  [MPa]) and leaf water potential ( $\psi_l$  [MPa]) and mediated by the bulk conductance along the flowpath ( $g_{sp}(\psi)$  [mm day<sup>-1</sup> MPa<sup>-1</sup>]). For simplicity, we assume constant soil-plant conductance ( $g_{sp}$ ) and ignore its dependence on water potential (i.e., hydraulic limits (Sperry et al., 1998)). This assumption simplifies the integral in Eq. 1 to the product of  $g_{sp}$  and the water potential difference,  $\psi_s - \psi_l$ , which drives the flow.

$$T_s = - \int_{\psi_s}^{\psi_l} g_{sp}(\psi) d\psi = g_{sp} \cdot (\psi_s - \psi_l) \quad (1)$$

The minimalist PHM demand ( $T_d$  [mm day<sup>-1</sup>]; Eq. 2 and red segment in Fig. 1a) uses a similar conductance-difference formulation (i.e. integrated flux-gradient relationship). Transpiration is driven by the leaf-to-air water vapor pressure deficit ( $D$  [mol H<sub>2</sub>O/mol air]) and mediated by the well-watered stomatal conductance ( $g_{s,ww}$  [mol air m<sup>-2</sup> s<sup>-1</sup>]), a stomatal closure

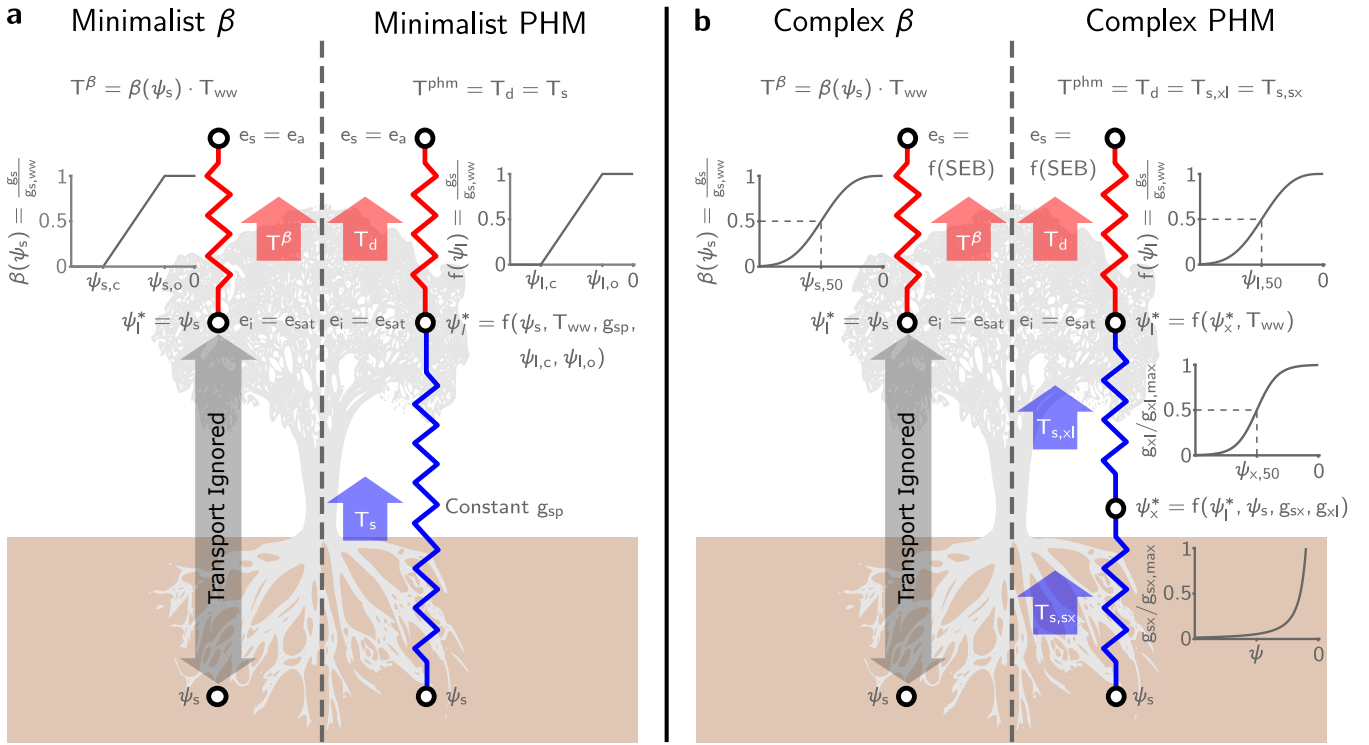


**Figure 1.** Schematic for the minimalist and complex  $\beta$  and PHM models used in this analysis. The resistors represent the conductance between soil-plant segments (i.e., an analogy to Ohm's Law) that mediate liquid water supply (blue) and atmospheric water vapor demand (red). Next to each resistor the segment-specific conductance downregulation curve dependent on water potential ( $\psi$ ). The white circles indicate segment endpoints where we calculate the potentials ( $\psi$ ) for liquid water transport and vapor pressures ( $e$ ) for water vapor transport. The segment subscripts represent soil (s), xylem (x), leaf (l), inside the leaf (i) and ambient air (a). For water vapor transport, we assume saturation vapor pressure inside the leaf ( $e_i = e_{sat}$ ). Furthermore, we assume the leaf surface vapor pressure ( $e_s$ ) is the atmospheric vapor pressure ( $e_a$ ) for the minimalist model, while  $e_s$  is a function of the surface energy balance ( $f(SEB)$ ) calculations at each time step for the complex formulation. is a function of the surface energy budget solution at each time step. The thick arrows represent the water transport through each segment calculated by the integrated, steady-state flux-gradient relationships discussed in Sect. 2.1-2.2 and Sect. 2.5. We use the minimalist models (left panel) for Sect. 3.1-3.2 and the complex models (right panel) for the LSM analysis in Sect. 3.3 (Note: We only illustrate a single-leaf formulation here, but see Sect. S2 for full details of the two-leaf implementation.).

90 term ( $f(\psi_l)$ ), and the leaf area index ( $LAI$  [ $\text{m}^2$  leaf  $\text{m}^{-2}$  ground]). Additionally, we convert  $T_d$  from a molar flux to a volume flux using the conversion factor  $C_a$  (i.e., molar weight of water ( $M_w$  [ $\text{kg mol}^{-1}$ ]) divided by water density ( $\rho_w$  [ $\text{kg m}^{-3}$ ]) and multiplied by the conversion from  $\text{m s}^{-1}$  to  $\text{mm day}^{-1}$ ). The driving force  $D$  assumes saturation vapor pressure inside the leaf (i.e.,  $e_i = e_{sat}$ ) and that the leaf surface ( $e_s$ ) and atmospheric vapor pressure ( $e_a$ ) are the same. The parameter  $g_{s,ww}$  encapsulates the stomatal response to atmospheric conditions only (i.e., light, temperature, humidity, and  $\text{CO}_2$  concentration).

95 We define the product of  $LAI$ ,  $g_{s,ww}$  and  $D$  as the well-watered transpiration rate ( $T_{ww}$ )—which represents atmospheric

moisture demand throughout this paper— and specify its value for the minimalist analysis. The term ‘well-watered’ refers to abundant soil water conditions under which water transport to the leaves maintains  $\psi_l$  high enough to avoid stomatal closure. During water-stressed conditions, the  $f(\psi_l)$  term represents stomatal closure (i.e., downregulating  $g_{s,ww}$ ) to lowering leaf water status (Buckley, 2019). We assume a normalized, piecewise linear  $f(\psi_l)$  (Eq. 3 and illustrated in Fig. 1a), parametrized by the leaf water potential at incipient ( $\psi_{l,o}$ ) and complete stomatal closure ( $\psi_{l,c}$ ). This simple multiplicative reduction of  $g_{s,ww}$  (similar to the approach of Jarvis (1976)) captures the observed non-unique relationship between  $g_s$  and  $\psi_l$  (Anderegg and Venturas, 2020) while facilitating comparison with the similar minimalist  $\beta$  formulation (see Sect. 2.5).

$$T_d = LAI \cdot f(\psi_l) \cdot g_{s,ww} \cdot D \cdot C_a = f(\psi_l) \cdot T_{ww} \cdot C_a \quad (2)$$

$$f(\psi_l) = \frac{g_s(\psi_l)}{g_{s,ww}} = \begin{cases} 1 & \psi_l \geq \psi_{l,o} \\ \frac{\psi_{l,c} - \psi_l}{\psi_{l,c} - \psi_{l,o}} & \psi_{l,c} < \psi_l < \psi_{l,o} \\ 0 & \psi_l \leq \psi_{l,c} \end{cases} \quad (3)$$

The PHM supply and demand are coupled through their mutual dependence on leaf water potential. The  $\psi_l$  value that balances supply (Eq. 1) and demand (Eq. 2)—which we will call  $\psi_l^*$  (Eq. 4)—yields the steady state transpiration rate for the minimalist PHM ( $T^{phm}$ ; Eq. 5). The full derivation of  $\psi_l^*$  and  $T^{phm}$  is shown in Sect. S1.

$$\psi_l^* = \frac{\psi_s \cdot (\psi_o - \psi_c) + \frac{T_{ww} \cdot \psi_c}{g_{sp}}}{(\psi_o - \psi_c) + \frac{T_{ww}}{g_{sp}}} \quad (4)$$

$$T^{phm} = \begin{cases} T_{ww} & \psi_s > \psi_{l,o} + \frac{T_{ww}}{g_{sp}} \\ T_{ww} \cdot \frac{(\psi_{l,c} - \psi_s)}{(\psi_{l,c} - \psi_{l,o}) - \frac{T_{ww}}{g_{sp}}} & \psi_{l,c} < \psi_s \leq \psi_{l,o} + \frac{T_{ww}}{g_{sp}} \\ 0 & \psi_s \leq \psi_{l,c} \end{cases} \quad (5)$$

## 2.2 Complex PHM

The LSM analysis (Sect. 3.3) uses a more complex PHM formulation following Feng et al. (2018). The PHM separates supply into soil-to-xylem and xylem-to-leaf segments and demand into a leaf-to-atmosphere segment (Fig. 1b). Here, we briefly discuss the complex PHM components for a single big-leaf formulation; however, we refer the reader to Sect. S2-S3 for full model details and parameter values for the two big-leaf formulation used in our LSM.

For PHM supply ( $T_s$ ; blue segments in Fig. 1b), the water potential gradient drives flow through the soil-plant system mediated by the segment-specific conductance. Unlike the minimalist PHM (Sect. 2.1), we assume the conductance in each segment depends on water potential, which represents ‘hydraulic limits’ (Sperry et al., 1998) that arise via (i) the inability of

roots to remove water from soil pores at low  $\psi_s$  and (ii) xylem embolism caused by large hydraulic gradients required under low  $\psi_s$  and/or high  $T_{ww}$ . The soil-to-xylem conductance ( $g_{sx}$  [mm day<sup>-1</sup> MPa<sup>-1</sup>]; Eq. 6 and illustrated in Fig. 1b) is its maximum value ( $g_{sx,max}$ ) downregulated by the unsaturated soil hydraulic conductivity curve (Clapp and Hornberger, 1978), which is parametrized by the saturated soil water potential ( $\psi_{sat}$ ), soil water retention exponent ( $b$ ), unsaturated hydraulic conductivity exponent ( $c = 2b + 3$ ), and a correction factor ( $d$ ) to account for roots' ability to reach water (Daly et al., 2004). The xylem-to-leaf conductance ( $g_{xl}$  [ms<sup>-1</sup> MPa<sup>-1</sup>]; Eq. 7 and illustrated in Fig. 1b) is its maximum value ( $g_{xl,max}$ ) downregulated by a sigmoidal function (Pammenter and Willigen, 1998), which is parametrized by the vulnerability exponent ( $a$ ) and the xylem water potential ( $\psi_x$ ) at 50% loss of conductance ( $\psi_{x,50}$ ). We estimate the maximum conductance values for each segment ( $g_{sx,max}$  and  $g_{xl,max}$ ) with trait-based equations following Feng et al. (2018) (see Sect. S2.5.3). Given that conductance varies with water potential, we utilize a Kirchhoff transform (Eq. 8) to approximate the water supply from each segment ( $T_{s,sx}$  and  $T_{s,xl}$  [mm day<sup>-1</sup>]; Eq. 9-10) as the difference in the matric flux potential ( $\Phi$  [mm day<sup>-1</sup>]) at the segment endpoints. Therefore, given a value of  $\psi_s$  (i.e., root zone average potential) and  $\psi_l$ , the  $\psi_x$  that balances  $T_{s,sx}$  and  $T_{s,xl}$ —called  $\psi_x^*$ —yields the steady-state supply rate ( $T_s$ ).

$$g_{sx}(\psi) = g_{sx,max} \cdot \left( \frac{\psi_{sat}}{\psi} \right)^{\frac{c-d}{b}} \quad (6)$$

$$g_{xl}(\psi) = g_{xl,max} \cdot \left[ 1 - \frac{1}{1 + e^{a(\psi - \psi_{x,50})}} \right] \quad (7)$$

$$\Phi(\psi) = \int_{-\infty}^{\psi} g(\psi') d\psi' \quad (8)$$

$$T_{s,sx} = \Phi_{sx}(\psi_s) - \Phi_{sx}(\psi_x) \quad (9)$$

$$T_{s,xl} = \Phi_{xl}(\psi_x) - \Phi_{xl}(\psi_l) \quad (10)$$

The complex PHM demand ( $T_d$  [mm day<sup>-1</sup>]; Eq. 11 and red segment in Fig. 1b) mirrors the minimalist version (Eq. 2) with modifications to fit into a dual-source LSM scheme (Sect. 2.3) that explicitly represents the coupled mass, heat and energy transfer between the plant and its microclimate and the atmosphere. The driving force of transpiration is no longer  $D$  but rather the difference between leaf internal ( $e_i$  [kPa]) and surface ( $e_s$  [kPa]) vapor pressure (normalized by atmospheric pressure ( $P_{atm}$  [kPa]) to obtain units mol H<sub>2</sub>O/mol air). We still assume  $e_i$  is the saturation vapor pressure at leaf temperature ( $e_{sat}$ ), but  $e_s$  depends on the plant microclimate determined by the LSM energy balance solution at each time step (see Sect. S2.6). This

plant microclimate is coupled to the well-watered stomatal conductance ( $g_{s,ww}$  [mol air m<sup>-2</sup> s<sup>-1</sup>]) via the optimality-based stomatal response model of Medlyn et al. (2011). The Medlyn model (Eq. 12) depends on the leaf vapor pressure difference ( $e_i - e_s$  [kPa]), net CO<sub>2</sub> assimilation rate ( $A_n$  [mol CO<sub>2</sub> m<sup>-2</sup> s<sup>-1</sup>]), and the leaf surface CO<sub>2</sub> mole fraction (approximated by the ratio of leaf surface CO<sub>2</sub> partial pressure ( $c_s$  [kPa]) and  $P_{atm}$  to give units [mol CO<sub>2</sub>/mol air]) and is parametrized by the minimum stomatal conductance ( $g_o$  [mol air m<sup>-2</sup> s<sup>-1</sup>]) and a slope parameter ( $g_1$  [kPa<sup>0.5</sup>]). Furthermore, we couple  $g_{s,ww}$  to the Farquhar et al. (1980) photosynthesis model through  $A_n$  to ensure CO<sub>2</sub> diffusion into the leaf balances carbon assimilation (Collatz et al., 1991) (see Sect. S2.4). As in the minimalist model, the product of  $g_{s,ww}$ , driving force, and  $LAI$  yields the well-watered transpiration rate,  $T_{ww}$ , which we take to represent atmospheric moisture demand. Under water-stressed conditions, we keep a Jarvis-like stomatal closure term ( $f(\psi_l)$ ) to downregulate  $g_{s,ww}$  because it facilitates easy comparisons between our minimalist and complex formulations. However, we upgrade  $f(\psi_l)$  from a piecewise linear form (Eq. 3) to a more realistic Weibull form (Eq. 13 and illustrated in Fig. 1b) parametrized by a shape factor ( $b_l$ ) describing stomatal sensitivity and the leaf water potential at 50% loss of conductance ( $\psi_{l,50}$  [MPa]) (Klein, 2014; Kennedy et al., 2019).

$$T_d = LAI \cdot f(\psi_l) \cdot g_{s,ww} \cdot \frac{e_i - e_s}{P_{atm}} \cdot C_a = f(\psi_l) \cdot T_{ww} \cdot C_a \quad (11)$$

$$g_{s,ww} = g_o + \left(1 + \frac{g_1}{\sqrt{e_i - e_s}}\right) \cdot \frac{1.6 \cdot A_n}{c_s / P_{atm}} \quad (12)$$

$$f(\psi_l) = \frac{g_s(\psi_l)}{g_{s,ww}} = 2^{-\left(\frac{\psi_l}{\psi_{l,50}}\right)^{b_l}} \quad (13)$$

As in the minimalist PHM, the complex PHM supply and demand are coupled through their mutual dependence on  $\psi_l$ . The  $\psi_l^*$  that balances  $T_s$  (found at  $\psi_x^*$  for Eq. 9-10) and  $T_d$  (Eq. 11) yields the steady-state transpiration rate for the complex PHM ( $T^{phm}$ ). We numerically calculate this solution by recasting Eq. 9-11 as a nonlinear least squares problem and finding the  $\psi_l^*$  and  $\psi_x^*$  that ensure mass balance between the segments (see Sect. S2.5.3).

### 2.3 LSM Description and Calibration

We created an LSM to allow testing of several transpiration downregulation schemes (Sect. 3.3) and removal of modules (e.g. subsurface heat and mass transfer) that would unnecessarily complicate our comparisons. Our LSM is a dual-source, two big-leaf approximation (Bonan, 2019) adapted from CLM v5 (Oleson et al., 2018) with several key simplifications: i) steady-state conditions (i.e., no above ground mass, heat or energy storage), ii) neutral atmospheric stability, iii) implemented the Goudriaan and Laar (1994) radiative transfer model in lieu of the two-stream approximation (Oleson et al., 2018), and iv) forced LSM with soil moisture, soil heat flux and down-welling radiation data. We refer the reader to Sect. S2 for full model details and justifications. We formulated the LSM in MATLAB and have made the codes available online.

We created separate LSM versions to test five different transpiration downregulation schemes: i) well-watered (no down-  
 170 regulation), ii) a single  $\beta$  ( $\beta_s$ ) with static parameters, iii) a  $\beta$  separately applied to sunlit and shaded leaf areas ( $\beta_{2L}$ ) with  
 static parameters, iv) a ‘dynamic  $\beta$ ’ with parameters dependent on  $T_{ww}$  ( $\beta_{dyn}$ ), and v) a PHM. We calibrated the PHM version  
 using a two-step approach. First, we simulated 13,600 parameter sets using Progressive Latin Hypercube Sampling (Razavi  
 et al., 2019) on 15 soil and plant parameters (Table S6) and selected the best parameter set based on a comparison of RMSE,  
 correlation coefficient, percent bias and variance to Ameriflux evapotranspiration, sensible heat flux, gross primary productiv-  
 175 ity, and net radiation site data (Fig. S5-S8). Unfortunately, the best parameter set contained an unrealistically low  $\psi_{l,50}$  value  
 for ponderosa pine compared to observations (DeLucia and Heckathorn, 1989). Therefore, as a second step, we adjusted the  
 $\psi_{l,50}$  and several other soil and plant parameters to more realistic values while ensuring that they replicate the transpiration  
 downregulation behavior of the original parameter set. These parameter adjustments had minimal impact on LSM predictions  
 as the underlying equations are highly nonlinear and multiple parameter sets can give near equivalent results (i.e., equifinality).  
 180 We refer the reader to Sect. S4 for a more detailed account of calibration.

We parametrized the three LSM versions containing the  $\beta$  schemes by calibrating the respective  $\beta$  functions to the relative  
 transpiration outputs ( $T/T_{ww}$ ) of the calibrated PHM version, while we ran the well-watered version using the calibrated pa-  
 rameters and downregulation turned off. The choice to calibrate a single LSM version ensured that the performance differences  
 between the schemes would be due to the PHM representing plant water use more realistically and not to the artifact of differ-  
 185 ing parameter fits between LSM versions. We refer the reader to Sect. S6.2 for specific details of the parameter fits for the  $\beta$   
 schemes.

## 2.4 Site Description and Forcing Data

We calibrated and forced the LSM with half-hourly data from the US-Me2 “Metolius” Ameriflux site (Irvine et al., 2008).  
 The site consists of intermediate-age ponderosa pine trees on sandy loam soil in the Metolius River Basin in Oregon, USA.  
 190 We selected this site specifically for its subsurface soil moisture and temperature profiles as well as its separate measurements  
 of photosynthetically active radiation (PAR) and near infrared radiation (NIR). We used these boundary condition data to  
 force the LSM in lieu of solving one-dimensional mass and heat transfer equations and atmospheric radiation partitioning  
 models. In particular, we forced the LSM with root zone averaged soil water potential ( $\psi_s$ ; estimated from measured soil water  
 content and a pedotransfer function) and the ground heat flux measurements. We selected the measurement depth of 50 cm  
 195 to represent  $\psi_s$  based on the deviation of measured  $GPP$  from its mean in relation to measured soil water content and vapor  
 pressure deficit (Fig. S10). The 50 cm measurements showed clear  $GPP$  downregulation under water stress. Furthermore, the  
 depth seemed reasonable given previous modeling at this site estimated an effective rooting depth of 1.1 m (Schwarz et al.,  
 2004). The atmospheric forcing for the LSM consisted of incoming direct and diffuse NIR and PAR fluxes,  $CO_2$  concentration,  
 atmospheric pressure, vapor pressure, temperature and wind velocity at the measurement tower height of 32 m. Full description  
 200 of the forcing data is given in Sect. S5.

## 2.5 $\beta$ Formulations

The  $\beta$  function empirically represents stomatal closure to declining leaf water status caused by soil water stress. By design,  $\beta$  makes the simplifying assumption that stomata respond directly to soil water status (to avoid the complexity of implementing a PHM shown in Fig. 1), which is readily available in TBM subsurface hydrology schemes as  $\psi_s$  or volumetric soil water content ( $\theta_s$ ). This heuristic approach leads to multiple  $\beta$  functions based on modeler preference (see Supplement of Trugman et al. (2018) for list of differing  $\beta$  formulations common to TBMs). Furthermore, even if a universal  $\beta$  function existed, there is open debate on how to apply the  $\beta$  factor (Egea et al., 2011); some TBMs apply the  $\beta$  factor directly to stomatal conductance (Kowalczyk et al., 2006; De Kauwe et al., 2015; Wolf et al., 2016) whereas others indirectly affect stomatal conductance by applying the  $\beta$  factor to photosynthetic parameters (Zhou et al., 2013; Lin et al., 2018; Kennedy et al., 2019). Here, we select a single  $\beta$  formulation that easily compares with the demand component of our PHM. Selecting a different  $\beta$  formulation could alter our values; however, we do not expect our main conclusions about  $\beta$  and PHM differences to change as long as two criteria are met. First, the stomatal downregulation factors for the PHM ( $f(\psi_l)$ ) and  $\beta$  ( $\beta(\psi_s)$ ) are applied consistently in the transpiration downregulation scheme (to either  $g_{s,ww}$  or photosynthetic parameters). Second, if  $\beta$  is in terms of  $\theta_s$ , a curvilinear form must be used (Egea et al., 2011) to ensure  $\beta$  can be mapped approximately to the water potential space of our analysis.

In this paper, we have defined the  $\beta$  function in terms of  $\psi_s$  and apply the  $\beta$  factor directly to  $g_{s,ww}$  and, in turn,  $T_{ww}$  (Eq. 14) for three key reasons: i) water transport through the soil-plant-atmosphere continuum follows a gradient of water potential, not water content, ii)  $\beta$  using  $\psi_s$  rather than  $\theta_s$  produces more realistic downregulation behavior compared to data (Verhoef and Egea, 2014), and iii) applying the  $\beta$  factor to  $g_{s,ww}$  directly corresponds to the PHM demand in both minimalist and complex formulations. In the minimalist analysis (Sect. 3.1-3.2),  $\beta(\psi_s)$  (Eq. 15 and illustrated in Fig. 1a) takes a piecewise linear form (analogous to Eq. 3) which is parametrized by the soil water potential at incipient ( $\psi_{s,o}$ ) and complete stomatal closure ( $\psi_{s,c}$ ). Similarly, in the LSM analysis (Sect. 3.3),  $\beta(\psi_s)$  (Eq. 16 and illustrated in Fig. 1b) takes a Weibull form (analogous to Eq. 13) parametrized by the soil water potential at 50% loss of stomatal conductance ( $\psi_{s,50}$ ) and a stomatal sensitivity parameter ( $b_s$ ). The LSM analysis uses two versions of Eq. 16: i) a static version with constant  $b_s$  and  $\psi_{s,50}$  (used by the  $\beta_s$  and  $\beta_{2L}$  schemes), and ii) a dynamic version where  $b_s$  and  $\psi_{s,50}$  are linear functions of  $T_{ww}$  (used by the  $\beta_{dyn}$  scheme). We refer the reader to Fig. S12 for illustrations of the different  $\beta$  versions.

$$T^\beta = \beta(\psi_s) \cdot T_{ww} \quad (14)$$

$$\beta(\psi_s) = \begin{cases} 1 & \psi_s \geq \psi_{s,o} \\ \frac{\psi_{s,c} - \psi_s}{\psi_{s,c} - \psi_{s,o}} & \psi_{s,c} < \psi_s < \psi_{s,o} \\ 0 & \psi_s \leq \psi_{s,c} \end{cases} \quad (15)$$

$$\beta(\psi_s, T_{ww}) = 2^{-\left(\frac{\psi_s}{\psi_{s,50}(T_{ww})}\right)^{b_s(T_{ww})}} \quad (16)$$

### 3 Results

#### 3.1 $\beta$ as a Limiting Case of PHMs with Infinite Conductance

The supply-demand framework reveals that the minimalist PHM and  $\beta$  fundamentally differ in their coupling of the effects of soil water stress (represented by  $\psi_s$ ) and atmospheric moisture demand (represented by  $T_{ww}$ ) on transpiration. The PHM supply lines (red lines in Fig. 2a) illustrate soil-to-leaf water transport (Eq. 1) at a fixed soil water availability ( $\psi_s$ ) under increasing pull from the leaf (lower  $\psi_l$ ) and constant soil-plant conductance ( $g_{sp}$ ; supply line slope). The PHM demand lines (black lines in Fig. 2a) illustrate transpiration reduction under lower  $\psi_l$  (from stomatal closure) for two  $T_{ww}$  values. The supply and demand lines intersect at the minimalist PHM solution ( $\psi_l^*$  and  $T^{phm}$ ; Eq. 4-5). Therefore, the minimalist PHM couples the effects of soil water stress to atmospheric moisture demand on transpiration downregulation because leaf water potential responds to  $\psi_s$  and  $T_{ww}$  until it reaches the point of steady-state transpiration (i.e.,  $T^{phm}(\psi_l^*) = T_s(\psi_l^*) = T_d(\psi_l^*)$ ).

The minimalist  $\beta$  transpiration rate ( $T^\beta$ , Eq. 14) ignores this coupling as the  $\beta$  function depends only on  $\psi_s$  and independently reduces  $T_{ww}$  (shown in Fig. 1). The conditions leading to the decoupling in  $\beta$  only arise if the supply lines are vertical (Fig. 2b), which results in the relative transpiration ( $T^\beta/T_{ww}$ ) depending on  $\psi_s$  only (single curve in Fig. 2d). Since  $g_{sp}$  is the supply line slope (Eq. 1),  $\beta$  represents a limiting case of the PHM in which the soil-plant system is infinitely conductive. More specifically, as  $g_{sp}$  increases, the leaf water potential approaches the soil water potential ( $\psi_l^* \rightarrow \psi_s$ ; Eq. 17) and the PHM transpiration rate approaches the  $\beta$  transpiration rate ( $T^{phm} \rightarrow T^\beta$ ; Eq. 18). Therefore, the  $\beta(\psi_s)$  function (Eq. 15) equals the  $f(\psi_l)$  function (Eq. 3) in PHMs and represents stomatal closure to declining leaf (or soil) water potential. In summary, the empirical  $\beta$  physically represents an infinitely conductive soil-plant system where stomata close in response to leaf water potential that depends solely on soil water potential with which it is equilibrated.

$$\lim_{g_{sp} \rightarrow \infty} [\psi_l^*] = \lim_{g_{sp} \rightarrow \infty} \left( \frac{\psi_s \cdot (\psi_o - \psi_c) + \frac{T_{ww} \cdot \psi_c}{g_{sp}}}{(\psi_o - \psi_c) + \frac{T_{ww}}{g_{sp}}} \right) = \psi_s \quad (17)$$

$$\lim_{g_{sp} \rightarrow \infty} (\Delta T) = \lim_{g_{sp} \rightarrow \infty} (T^{phm} - T^\beta) = \lim_{g_{sp} \rightarrow \infty} \left( T_{ww} \cdot \left[ \frac{(\psi_{l,c} - \psi_s)}{(\psi_{l,c} - \psi_{l,o}) - \frac{T_{ww}}{g_{sp}}} - \frac{(\psi_{l,c} - \psi_s)}{(\psi_{l,c} - \psi_{l,o})} \right] \right) = 0 \quad (18)$$

The PHM coupling results in greater transpiration downregulation compared to  $\beta$  under the same environmental conditions (Fig. 2c). For a given soil water stress ( $\psi_s$ ),  $\beta$  assumes  $\psi_s = \psi_l^*$  and downregulates any atmospheric moisture demand ( $T_{ww}$ ) value a fixed proportion (i.e., it scales linearly with  $T_{ww}$ ); hence, it can be modeled with a single curve (Fig. 2d). Conversely, the PHM (with finite conductance) requires a water potential difference ( $\Delta\psi = \psi_s - \psi_l^*$ ) to transport water from soil-to-leaf; therefore,  $\psi_l^*$  must be less than  $\psi_s$  and greater stomatal closure results (Fig. 2c). Furthermore, the PHM downregulates transpiration at a greater proportion with increasing  $T_{ww}$  (i.e., it scales nonlinearly with  $T_{ww}$ ) as it requires a greater  $\Delta\psi$  and lower  $\psi_l^*$  (Fig. 2d). Hence, PHMs require transpiration downregulation to be described as a function of both  $\psi_s$  and  $T_{ww}$ .

These minimalist model results suggest that the range of soil-plant conductances ( $g_{sp}$ ) can generate a spectrum of possible transpiration responses to soil water stress (and atmospheric moisture demand). Two classes of behaviors emerge—one in

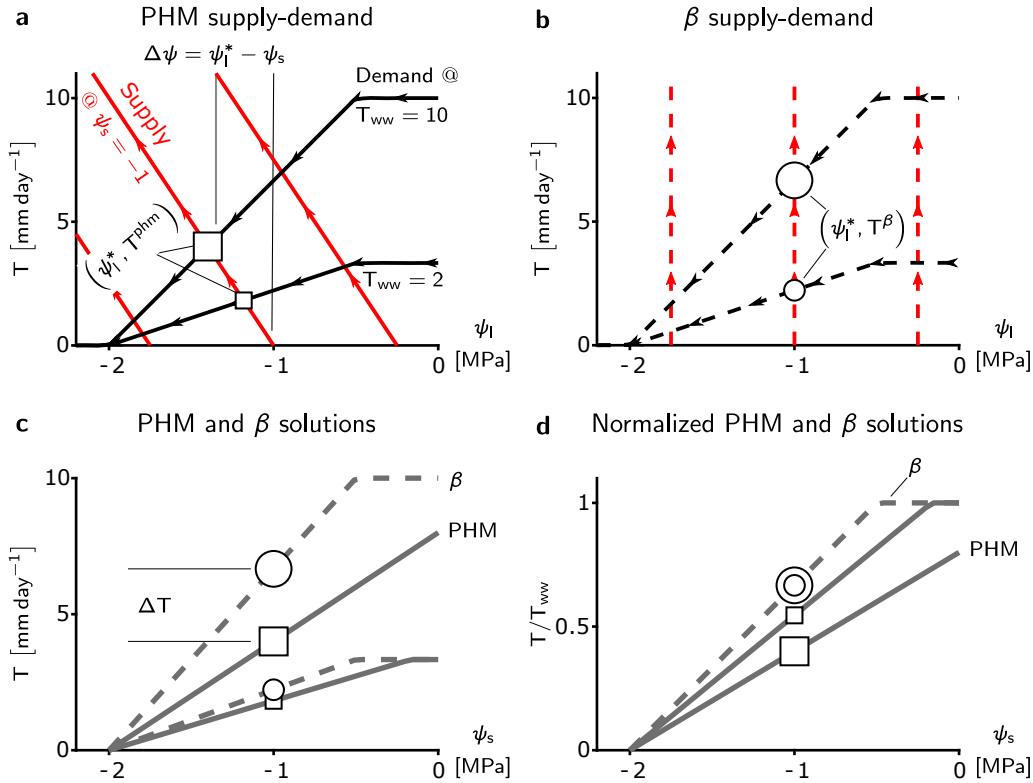


**Figure 2.** Fundamental differences between minimalist PHM and  $\beta$ . **a-b**, Supply (red) and demand (black) curves for PHM (**a**, solid lines) and  $\beta$  (**b**, dashed lines) under varying leaf water potentials ( $\psi_l$ ). The squares (circles) represent the PHM ( $\beta$ ) solution — i.e., the  $\psi_l^*$  where supply equals demand — for a single soil water availability ( $\psi_s$ ) and two atmospheric moisture demands ( $T_{ww}$ ). These markers carry through panels **c** and **d** to illustrate how the solutions between the PHM and  $\beta$  diverge at a single  $\psi_s$ . The relative size of the markers indicates corresponding  $T_{ww}$ . The water potential difference  $\Delta\psi$  required to transport water from soil to leaf is shown in panel **a** for  $\psi_s = -2$  MPa and  $T_{ww} = 10$  mm day<sup>-1</sup>. **c**, Solutions of panels **a** and **b** mapped to  $\psi_s$ , where  $\Delta T$  is the difference between PHM and  $\beta$  transpiration estimates at  $\psi_s = -2$  MPa and  $T_{ww} = 10$  mm day<sup>-1</sup>. **d**, Relative transpiration, in which solutions in panel **c** are normalized by  $T_{ww}$ . The  $\beta$  solutions collapse to a single curve, whereas the PHM solutions depend on  $T_{ww}$ .

260 a ‘soil-limited’ soil-plant system, in which  $g_{sp}$  is large enough for  $\psi_l \approx \psi_s$ , thus decoupling the effects of soil water stress and atmospheric moisture demand while allowing the relative transpiration to vary only with  $\psi_s$  (Fig. 2d). The other class of behavior arises in ‘transport-limited’ systems with finite  $g_{sp}$ , in which a non-negligible water potential difference ( $\Delta\psi$ ) is required to transport the water to the leaf, resulting in additional downregulation compared to soil-limited systems (Fig. 2d) and requiring relative transpiration to depend on both  $\psi_s$  and  $T_{ww}$ .

The differences in PHM and  $\beta$  transpiration estimates ( $\Delta T$ ) depends not only on  $g_{sp}$ , but also on soil water availability ( $\psi_s$ ), atmospheric moisture demand ( $T_{ww}$ ) and plant water use strategy ( $\psi_{l,c} - \psi_{l,o}$ ). To disentangle these joint dependencies, we adjust a single variable and explore the impact on  $\Delta T$  using the supply and demand lines (Fig. 3). The translation of supply lines represents  $\psi_s$  changes (indicated in Fig. 3a,c,e) and produces a non-monotonic relationship with  $\Delta T$  over the range of soil water stress (i.e.,  $\psi_{l,c} < \psi_s < \psi_{l,o} + T_{ww}/g_{sp}$ ) (Fig. 3b,d,f). The peak  $\Delta T$  occurs at the incipient point of stomatal closure ( $\psi_{l,o}$ ) because i) when  $\psi_s < \psi_{l,o}$ , transpiration begins to decrease, and in its extreme limit, transpiration (and thus  $\Delta T$ ) approaches 0 and ii) when  $\psi_s > \psi_{l,o}$ , the effects of downregulation diminish in both models. The  $\Delta T$ - $\psi_s$  behavior acts as a baseline relationship in the following analysis of  $g_{sp}$ ,  $T_{ww}$ , and  $\psi_{l,c} - \psi_{l,o}$  controls.

The  $\Delta T$ - $\psi_s$  relationship increases with lower  $g_{sp}$  (Fig. 3b; greater transport-limitation) because flatter supply lines increase  $\Delta\psi$  (Fig. 3a), requiring greater stomatal closure and hence additional downregulation for a PHM compared to  $\beta$ . Similarly, higher  $T_{ww}$  increases  $\Delta T$ - $\psi_s$  relationship (Fig. 3d), although the increase in  $\Delta\psi$  stems from steeper demand line slope (Fig. 3c). In addition to increasing  $\Delta T$  at each  $\psi_s$  value, the effects of  $g_{sp}$  and  $T_{ww}$  increase the range of soil water stress above  $\psi_{l,o}$  (up to saturated soil water potential). This result indicates that PHMs can model transpiration downregulation under moist soil conditions that  $\beta$  potentially misses as it does not account for large  $\Delta\psi$  values from transport-limitation and/or high atmospheric moisture demand. Finally, as  $g_{sp}$  increases (soil-limited) and  $T_{ww}$  decreases,  $\Delta T$  tends to zero, once again, for slightly different reasons: for  $g_{sp}$ , the supply lines approach the  $\beta$  assumption (vertical dashed lines in Fig. 3a), whereas for  $T_{ww}$ , transpiration approaches zero.

Lastly, we explore the effect of plant water use strategy ( $\psi_{l,c} - \psi_{l,o}$ )—which approximates the sensitivity of stomatal closure to  $\psi_l$ —on  $\Delta T$ . Altering  $\psi_{l,c} - \psi_{l,o}$  does not affect  $\Delta\psi$  like the other three variables; however, it modifies the range of soil water stress and redistributes  $\Delta T$  to conserve the total error over the range. For example, a more aggressive plant water use strategy—closing stomata over a narrower range of  $\psi_l$  and  $\psi_s$ —creates a narrower range of soil water stress with a more peaked  $\Delta T$ - $\psi_s$  relationship due to more vertical demand lines (Fig. 3e). Therefore, whether the plant water use strategy could amplify or diminish  $\Delta T$  for a soil-system relies on how site-specific soil moisture variability overlaps with the range of soil water stress (Fig. 3f).

In summary, this minimalist analysis suggest PHMs are most needed to represent transport-limited soil-plant systems under high atmospheric moisture demand and moderate soil water availability. Plant water use will modulate these results; however, the impact depends on how site-specific soil moisture variability overlaps with the range of soil water stress.

### 3.3 Improving Transpiration Predictions with a PHM and a ‘Dynamic $\beta$ ’

We now perform a modeling case study of the Ameriflux US-Me2 ponderosa site (Sect. 2.4) using our own calibrated LSM (Sect. 2.3) with five separate transpiration downregulation schemes: i) well-watered (no downregulation), ii) single  $\beta$  ( $\beta_s$ ), iii)  $\beta$  separately applied to sunlit and shaded leaf areas ( $\beta_{2L}$ ), iv)  $\beta_{dyn}$ , and v) PHM. Specifically we aim to i) validate the transport-limitation spectrum (Sect. 3.1) for a more complex PHM formulation common to TBMs, ii) identify errors incurred

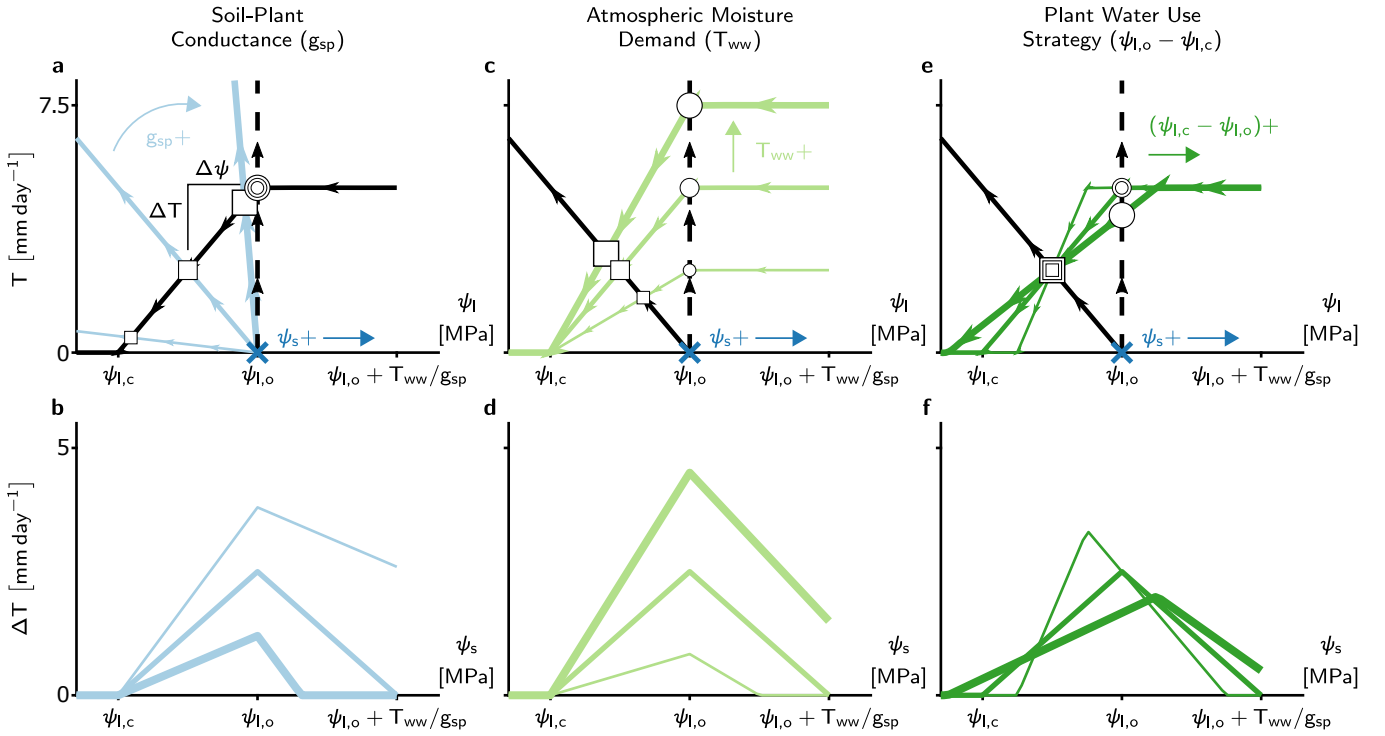


**Figure 3.** The effect of soil water potential ( $\psi_s$ ), soil-plant conductance ( $g_{sp}$ ), atmospheric moisture demand ( $T_{ww}$ ) and plant water use strategy ( $\psi_{l,o} - \psi_{l,c}$ ) on differences between the minimalist PHM and  $\beta$  models ( $\Delta T$ ). **a,c,e**, Supply-demand curves at a single soil water availability (indicated by the dark blue x at  $\psi_s = \psi_{l,o}$ ), for three prescribed values of  $g_{sp}$ ,  $T_{ww}$ , and  $\psi_{l,o} - \psi_{l,c}$ , respectively. Each parameter ( $g_{sp}$ ,  $T_{ww}$ , or  $\psi_{l,o} - \psi_{l,c}$ ) is set at 50% above (below) its base values at  $g_{sp} = 10 \text{ mm day}^{-1} \text{ MPa}^{-1}$ ,  $T_{ww} = 5 \text{ mm day}^{-1}$ ,  $\psi_o = -1 \text{ MPa}$ , and  $\psi_o = -2 \text{ MPa}$  using thick (thin) colored lines. The squares (circles) indicate the PHM ( $\beta$ ) solutions, with size corresponding to magnitude of the changing parameter values. Note: the vertical distance between correspondingly sized circle and square is  $\Delta T$  and horizontal distance is  $\Delta\psi$ . **b,d,f**, The  $\Delta T$  results from the panels **a**, **c**, and **e** calculated for a range of  $\psi_s$  with line thickness proportional to parameters in the aforementioned panels (e.g., thick blue line in panel **b** corresponds to 50% increase in  $g_{sp}$  shown in panel **a**). The x-axes are mapped from  $\psi_l$  in the top panels to  $\psi_s$  in the bottom panels.

by selecting  $\beta$  over a PHM (Sect. 3.2) for a real transport-limited soil-plant system, and iii) develop a new ‘dynamic  $\beta$ ’ that approximates a PHM with simple modifications to the existing  $\beta$ .

300 To aid our comparison of LSM transpiration downregulation schemes, we must first verify that the spectrum of transport-limitation found in our minimalist analysis (Sect. 3.1) adequately describes the differences between PHMs and the  $\beta$  formulations common to TBMs. Our calibrated LSM uses a more complex PHM formulation (Sect. 2.2 and Fig. 1b) that partitions the soil-plant-atmosphere continuum into soil-to-xylem, xylem-to-leaf, and leaf-to-atmosphere segments, each with conductance curves that depend nonlinearly (e.g., sigmoidal or Weibull) on water potential. This added complexity does not affect the

305 spectrum of transport-limitation (Fig. 4). For clarity, we reiterate two main points from the minimalist PHM analysis found

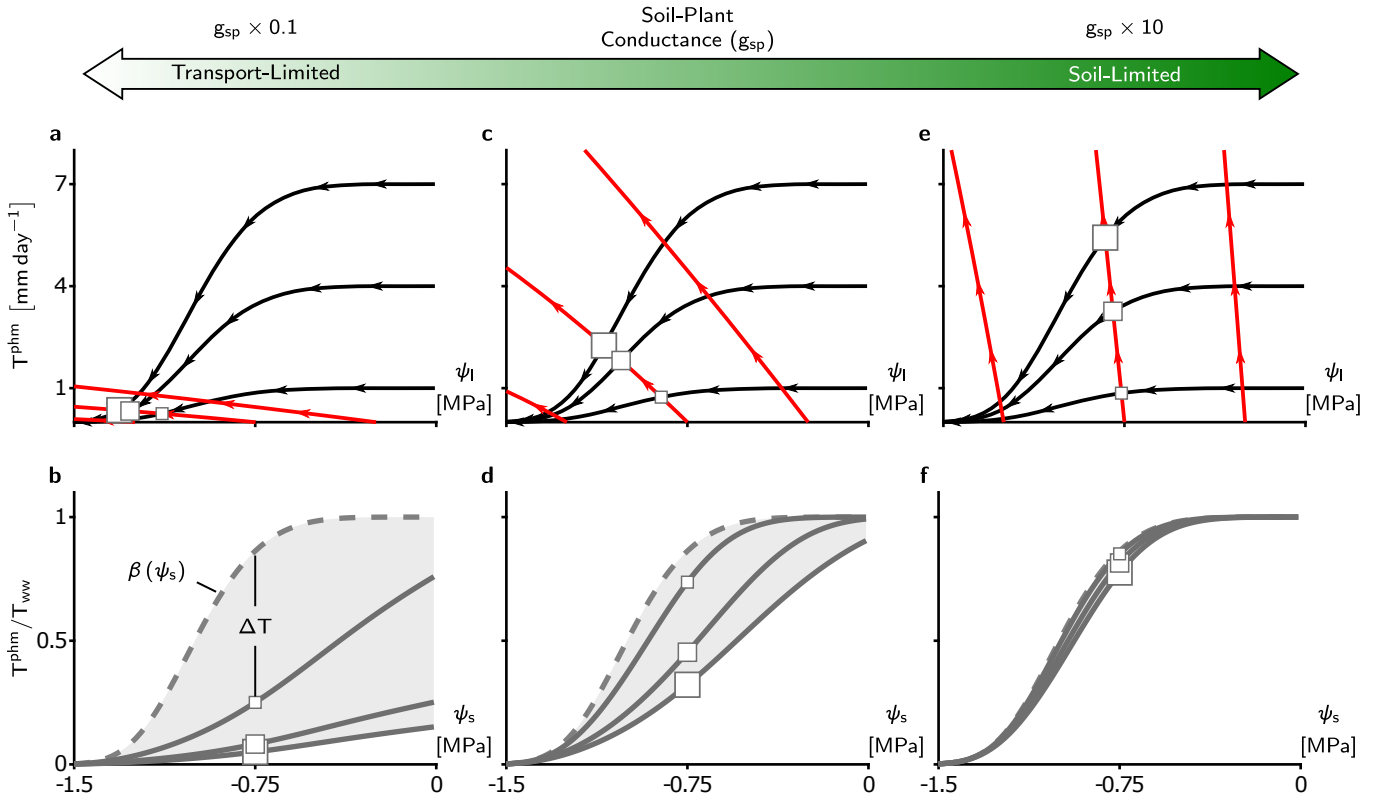


**Figure 4.** Transport-limitation spectrum observed in complex PHM formulation. **a,c,e**, Supply-demand curves for three values of soil-plant conductance,  $g_{sp}$ , using the more complex PHM formulation. Panel **c** is based on calibrated parameters ( $g_{sp} \approx 13 \text{ mm day}^{-1} \text{ MPa}^{-1}$ ) from the US-Me2 Ameriflux site containing mature ponderosa pines that were determined for the LSM analysis in this paper. Panels **a** and **e** contains the calibrated  $g_{sp}$  multiplied by 0.1 and 10, respectively. The supply lines (red) are shown at  $\psi_s$  equal to 0, -0.75, and -1.5 MPa and demand lines (black) are shown at  $T_{ww}$  equal to 1, 4, and 7  $\text{mm day}^{-1}$ . The PHM solution for  $\psi_s$  at -0.75 MPa is shown by the squares with size corresponding to  $T_{ww}$  magnitude. **b,d,f**, The relative transpiration for the PHM (solid) in panels **a**, **c**, and **e** and the infinitely conductive  $\beta$  solution (dashed line).

in this complex analysis. First, soil-plant conductance ( $g_{sp}$ ) controls whether the soil-plant system is soil-limited (high  $g_{sp}$ ; Fig. 4e-f) or transport-limited (low  $g_{sp}$ ; Fig. 4a-b) due to non-negligible water potential differences ( $\Delta\psi$ ) creating large differences between PHMs and  $\beta$  (high  $\Delta T$ ) at intermediate  $\psi_s$  values (Fig. 4b,d). Second, for a transport-limited system,  $\Delta T$  increases with higher variability in atmospheric moisture demand ( $T_{ww}$ ), where the importance of ‘variability’ expands on our

310 minimalist results. To clarify,  $\beta$  should be considered an empirical model that could be fit anywhere within the range of the PHM downregulation envelope (light gray shading in Fig. 4b,d,f). Therefore, greater  $T_{ww}$  variability creates a larger PHM downregulation envelope and makes a single  $\beta$  increasingly inadequate for modeling transpiration downregulation.

The consistency between the minimalist and more complex PHM suggests that the divergence between PHMs and  $\beta$  in transport-limited systems are not sensitive to the linear or nonlinear forms of supply or demand lines, but are rather controlled

315 by the existence of a finite conductance itself. Furthermore, these results strongly support the need to use two independent variables,  $\psi_s$  and  $T_{ww}$  (rather than only  $\psi_s$  in  $\beta$ ), to capture the coupled effects of soil water stress and atmospheric moisture demand on transpiration downregulation in transport-limited soil-plant systems. In light of these findings, we have developed a new ‘dynamic  $\beta$ ’ ( $\beta_{dyn}$ ) that has an additional functional dependence on  $T_{ww}$  (Eq. 16) and compared it against four other downregulation schemes in this LSM analysis.

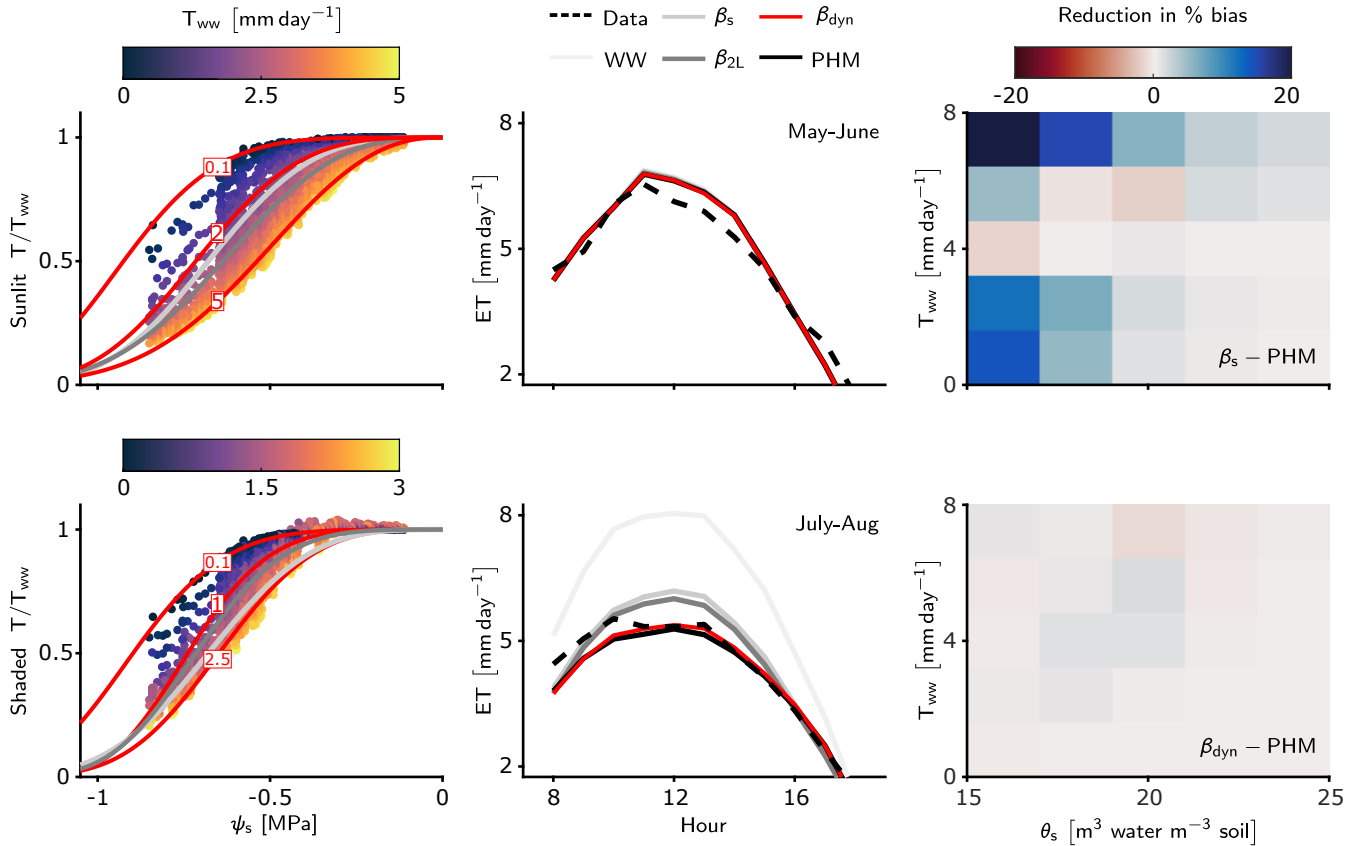


**Figure 5.** LSM evapotranspiration estimates improved by PHM and new ‘dynamic  $\beta$ ’. **a-b**, Fits of the  $\beta_s$ ,  $\beta_{2L}$ , and  $\beta_{dyn}$  schemes to the relative transpiration outputs from the calibrated PHM scheme for the sunlit (**a**) and shaded big-leaf (**b**) of the LSM (see Methods). Note that only three of the infinite family of  $\beta_{dyn}$  curves are shown for illustration. Full fitting details of these three schemes are available in Sect. S2. **c-d**, The median diurnal ET estimates for the LSM with five transpiration downregulation schemes compared to Ameriflux observations at the US-Me2 site for early (**c**) and late summer (**d**). The dual source LSM calculates ET as the sum of sunlit and shaded big-leaf transpiration and ground evaporation. Note:  $\beta_{dyn}$  (red) is overlying PHM (black) results as they are essentially the same. **e-f**, Reduction in absolute percent bias of ET between the  $\beta_s$  and PHM schemes (**e**) and  $\beta_{dyn}$  and PHM schemes (**f**) in terms of atmospheric moisture demand (represented by  $T_{ww}$ ) and soil water status (represented by  $\theta_s$ ). In both plots, blue indicates PHM improvement over the selected  $\beta$  scheme.

320 We now assess the errors incurred by using a  $\beta$  rather than PHM downregulation scheme to model the US-Me2 ponderosa pine site. The median diurnal evapotranspiration (ET; bare soil evaporation plus transpiration) for each LSM version for early

summer 2013-2014 (Fig. 5c-d) indicates that all downregulation schemes perform similarly due to high soil moisture and minimal downregulation (Fig. 5c). However, as soil moisture declines during late summer (Fig. S11) the differences between schemes emerge: the PHM and  $\beta_{dyn}$  schemes fit the ET observations the best, while  $\beta_{2L}$ ,  $\beta_s$ , and well-watered schemes over-  
 325 predict ET (Fig. 5d). We explain the poor performance of the static  $\beta$  schemes by plotting the reduction in absolute percent bias between the  $\beta_s$  and PHM schemes (Fig. 5e) of soil water stress (represented by volumetric soil water content measurements at the site ( $\theta_s$  [m<sup>3</sup> water m<sup>-3</sup> soil])) and atmospheric moisture demand (represented by  $T_{ww}$  from the well-watered LSM version). The PHM scheme provides substantial percent bias reduction relative to the static  $\beta_s$  scheme under soil water stress ( $\theta_s < 0.2$ ) for above- and below-average  $T_{ww}$  values ( $T_{ww} \approx 4$  mm day<sup>-1</sup>). This result is true for both static  $\beta$  schemes ( $\beta_s$   
 330 and  $\beta_{2L}$ ) because they are fit to the average  $T_{ww}$  behavior over the simulation period (Fig. 5a-b and Sect. S6.2). Therefore, as  $T_{ww}$  becomes higher (lower) than the average, these static  $\beta$  schemes will overpredict (underpredict) transpiration. The PHM also improves performance during wetter soil conditions ( $\theta_s > 0.2$ ) with high  $T_{ww}$ —which do not represent typical ‘drought’ conditions—suggesting that PHMs capture transpiration downregulation that  $\beta$  potentially misses as it cannot account for large soil-plant potential differences ( $\Delta\psi$ ) under transport-limitation and/or high atmospheric moisture demand (similar to  
 335 Sect. 3.2). Lastly, the near average  $T_{ww}$  conditions lead to  $\beta$  providing enhanced performance, which can be explained by underlying biases in the calibrated parameter estimates (see Fig. S9).

Notably, the  $\beta_{dyn}$  downregulation scheme replicates the performance of the PHM scheme by adding a single dimension of  $T_{ww}$  to the original  $\beta$  scheme. This additional dependence on  $T_{ww}$  allows  $\beta_{dyn}$  to traverse along the PHM downregulation envelope with atmospheric moisture demand changes, whereas the static  $\beta$  schemes are fixed near mean conditions (Fig. 5a-  
 340 b). The performance difference between PHM and  $\beta_{dyn}$  schemes is minimal in terms of percent change in bias across all environmental conditions (Fig. 5f), median diurnal variations (Fig. 5c-d), and cumulative flux errors (Table S7-S8). Therefore, this additional dependence on  $T_{ww}$  is key to simulating the coupled effects of atmospheric moisture demand and soil water stress in PHMs and accurately modeling transpiration downregulation in transport-limited systems. For this transport-limited system,  $\beta_{dyn}$  requires two more parameters than the original  $\beta$  scheme, which is half the parameters required for our complex  
 345 PHM formulation (Sect. S6.2). Furthermore,  $\beta_{dyn}$  does not require the iterative solution of water potentials and transpiration in PHMs (Sect. 2.2). Rather, it calculates transpiration downregulation algebraically using  $\psi_s$  as in the original  $\beta$ . The  $\beta_{dyn}$  provides a future avenue for correcting existing  $\beta$  model bias without adding the computational and parametric challenges of more realistic PHMs.

## 4 Discussion and Conclusion

350 The spectrum of transport-limited transpiration explains why many TBMs that use  $\beta$  to represent transpiration downregulation struggle to predict water, energy, and carbon fluxes under soil water stress (Sitch et al., 2008; Powell et al., 2013; Medlyn et al., 2016; Ukkola et al., 2016; Restrepo-Coupe et al., 2017; Trugman et al., 2018) and why implementing PHMs has led to performance improvements (Kennedy et al., 2019; Anderegg and Venturas, 2020; Eller et al., 2020; Sabot et al., 2020). Transpiration in a transport-limited soil-plant system, characterized by finite soil-plant conductance, depends on non-negligible

355 water potential differences to transport water from the soil to the leaf, which results from the joint effects of atmospheric moisture demand and soil water supply on leaf water potential. It is only when the soil-plant conductance becomes infinite (and the system becomes soil-limited) that leaf water potential approximates soil water potential, and transpiration arises as an independent function of soil water supply and atmospheric moisture demand. These are assumptions inherent to the empirical  $\beta$  and explains why  $\beta$  cannot capture the coupled effects of soil water stress and atmospheric moisture demand.

360 The implications of continued use of  $\beta$  will vary by site. Ecosystems with soil or plant hydraulic properties resistant to flow (e.g., xeric ecosystems, tall trees, species with low xylem conductivity or roots that hydraulically disconnects from the soil during drought) will have large biases depending on the range of soil water availability and atmospheric moisture demand ( $T_{ww}$ ) observed at the site (Fig. 3d and 4b). These errors will not be confined to drought periods, as higher atmospheric moisture demand and lower soil-plant conductance can result in errors even during wetter soil conditions (Fig. 3 and Fig. 5e).  
365 This is a crucial point, given projections indicate diverging degrees of VPD stress and soil water stress for ecosystems (Novick et al., 2016). On the other hand, for soil-limited systems (e.g., irrigated crops, riparian vegetation, or groundwater-dependent ecosystems),  $\beta$  may adequately capture transpiration dynamics as soil water status may be a suitable proxy for leaf water status. Therefore, further work must identify the combinations of soil parameters and plant hydraulic traits that define transport- or soil-limited systems to identify ecosystems susceptible to bias from  $\beta$ . Our initial estimates indicate a soil-plant conductance  
370 value around  $30 \text{ mm day}^{-1} \text{ MPa}^{-1}$  may be a rough threshold for transport-limitation (see Sect. S7).

Several other factors not covered in this work could exacerbate the differences between  $\beta$  and PHM predictions. We expect plant capacitance (already incorporated into some TBMs (Xu et al., 2016; Christoffersen et al., 2016)) will likely cause further deviations from  $\beta$ . PHMs with capacitance is expected to introduce hysteresis into transpiration downregulation (Zhang et al., 2014) in transport-limited systems that existing  $\beta$  are not equipped to capture. However, this hysteretic behavior may diminish  
375 in a high conductance (i.e., soil-limited) system because plant and soil water potentials will quickly equilibrate, so  $\beta$  may still be an adequate alternative to a PHM. More advanced representation of stomatal response and plant hydraulic transport could further exacerbate  $\beta$  and PHM differences. Recent advances in optimality-based (Eller et al., 2020; Sabot et al., 2020) and mechanistic stomatal response models (Buckley, 2017) as well as more detailed PHM segmentation (Kennedy et al., 2019) may include additional couplings to plant water and metabolism that cannot be easily approximated by  $\beta$ . Regardless, the core  
380 message of this work is still relevant: for transport-limited soil-plant systems, PHMs are necessary to couple the effects of soil water stress and atmospheric moisture demand on transpiration, and  $\beta$  fails because soil water status is not an adequate substitute for leaf water status.

The recognition that a ‘dynamic  $\beta$ ’ model can replicate the complexity of a PHM with half the parameters and more direct computation (Sect. S6.2), simply by adding a dependence on atmospheric moisture demand to the  $\beta$  function, provides a  
385 useful pathway for overcoming both the limitations of  $\beta$  and the parametric uncertainties of PHMs (Paschalis et al., 2020; Anderegg and Venturas, 2020). The inadequacies of the static  $\beta$  have been noted since its inception. Feddes et al. (1978), who introduced the first  $\beta$ , mentioned  $\beta$ ’s dependence on atmospheric moisture demand based on field data (Denmead and Shaw, 1962; Yang and de Jong, 1972) and early plant hydraulic theory (Gardner, 1960). Unfortunately, there have been only a few attempts to rectify these inadequacies in the modeling community, short of implementing a full PHM. For example,

390 Feddes and Raats (2004) updated their original  $\beta$  model to vary the water potential at incipient stomatal closure linearly with atmospheric moisture demand, which has been adopted in the field scale SWAP model (Kroes et al., 2017), while the Ecosystem Demography-2 model (Medvigy et al., 2009) uses a sigmoidal function for transpiration downregulation that contains the ratio of soil water supply to evaporative demand. Within many TBMs and hydrological models, a ‘dynamic  $\beta$ ’ could easily replace the original  $\beta$  by allowing existing fixed parameters to vary with  $T_{ww}$  (already calculated in many transpiration downregulation schemes). In addition to improving TBM performances, ‘dynamic  $\beta$ ’ also has the potential to aid in remote sensing retrievals and indirect inferences of land surface fluxes. Currently, the state-of-the-art ECOSTRESS satellite provides global ET estimates based on a modified Priestley-Taylor formulation that uses a  $\beta$  function to downregulate ET under soil water stress (Fisher et al., 2020). These satellite products could easily implement the ‘dynamic  $\beta$ ’ formulation to correct biases for many transport-limited ecosystems. These potential applications rely on formalizing the relationship between the ‘dynamic  $\beta$ ’ parameters and their dependence on  $T_{ww}$ . As it stands, the ‘dynamic  $\beta$ ’ still needs to be calibrated to site-specific data; however, it provides a physically-informed alternative to PHMs with less calculation and fewer parameters. Further work will focus on generalizing the ‘dynamic  $\beta$ ’ by linking its parameters to measurable soil properties, plant hydraulic traits, and atmospheric feedbacks.

*Code availability.*

*Author contributions.* X.F. and S.T. conceived the idea; B.P.S. and X.F. designed the research; B.P.S. performed the research; B.P.S. and X.F. wrote the paper; and S.T. contributed to refining results and revising the paper.

*Competing interests.* The authors declare no competing interests.

*Acknowledgements.* B.P.S. and X.F. acknowledge support from National Science Foundation award DEB-2045610. B.P.S. and X.F. also acknowledge the resources from The Minnesota Supercomputing Institute used to run the simulations in this work.

## References

- Anderegg, W. R. L.: Minireview Spatial and temporal variation in plant hydraulic traits and their relevance for climate change impacts on vegetation, *New Phytologist*, 205, 1008–1014, <https://doi.org/10.1111/nph.12907>, [www.newphytologist.com](http://www.newphytologist.com), 2015.
- Anderegg, W. R. L. and Venturas, M. D.: Plant hydraulics play a critical role in Earth system fluxes, *New Phytologist*, N/A, 4, <https://doi.org/10.1111/nph.16548>, <http://doi.wiley.com/10.1111/nph.16548>, 2020.
- Bohrer, G., Mourad, H., Laursen, T. A., Drewry, D., Avissar, R., Poggi, D., Oren, R., Katul, G. G., Bohrer, C. ., Mourad, H., Laursen, T. A.,  
415 Drewry, D., Avissar, R., Poggi, D., Oren, R., and Katul, G. G.: Finite element tree crown hydrodynamics model (FETCH) using porous media flow within branching elements: A new representation of tree hydrodynamics, 41, 11 404, <https://doi.org/10.1029/2005WR004181>, 2005.
- Bonan, G.: *Climate Change and Terrestrial Ecosystem Modeling*, Cambridge University Press, <https://doi.org/10.1017/9781107339217>, <https://www.cambridge.org/core/product/identifier/9781107339217/type/book>, 2019.
- 420 Bonan, G. B., Williams, M., Fisher, R. A., and Oleson, K. W.: Modeling stomatal conductance in the earth system: linking leaf water-use efficiency and water transport along the soil–plant–atmosphere continuum, *Geoscientific Model Development*, 7, 2193–2222, <https://doi.org/10.5194/gmd-7-2193-2014>, <https://www.geosci-model-dev.net/7/2193/2014/>, 2014.
- Buckley, T. N.: Modeling Stomatal Conductance, *Plant Physiology*, 174, 572–582, <https://doi.org/10.1104/pp.16.01772>, [www.plantphysiol.org/cgi/doi/10.1104/pp.16.01772](http://www.plantphysiol.org/cgi/doi/10.1104/pp.16.01772), 2017.
- 425 Buckley, T. N.: How do stomata respond to water status?, *New Phytologist*, 224, 21–36, <https://doi.org/10.1111/nph.15899>, <https://onlinelibrary.wiley.com/doi/abs/10.1111/nph.15899>, 2019.
- Buckley, T. N., Martorell, S., Diaz-Espejo, A., Tomàs, M., and Medrano, H.: Is stomatal conductance optimized over both time and space in plant crowns? A field test in grapevine (*Vitis vinifera*), <https://doi.org/10.1111/pce.12343>, <https://onlinelibrary.wiley.com/doi/pdf/10.1111/pce.12343>, 2014.
- 430 Christoffersen, B. O., Gloor, M., Fauset, S., Fyllas, N. M., Galbraith, D. R., Baker, T. R., Kruijt, B., Rowland, L., Fisher, R. A., Binks, O. J., Sevanto, S., Xu, C., Jansen, S., Choat, B., Mencuccini, M., McDowell, N. G., and Meir, P.: Linking hydraulic traits to tropical forest function in a size-structured and trait-driven model (TFS v.1-Hydro), *Geoscientific Model Development*, 9, 4227–4255, <https://doi.org/10.5194/gmd-9-4227-2016>, <https://www.geosci-model-dev.net/9/4227/2016/>, 2016.
- Clapp, R. B. and Hornberger, G. M.: Empirical equations for some soil hydraulic properties, *Water Resources Research*, 14, 601–604,  
435 <https://doi.org/10.1029/WR014i004p00601>, <http://doi.wiley.com/10.1029/WR014i004p00601>, 1978.
- Collatz, G., Ball, J., Grivet, C., and Berry, J. A.: Physiological and environmental regulation of stomatal conductance, photosynthesis and transpiration: a model that includes a laminar boundary layer, *Agricultural and Forest Meteorology*, 54, 107–136, [https://doi.org/10.1016/0168-1923\(91\)90002-8](https://doi.org/10.1016/0168-1923(91)90002-8), <https://www.sciencedirect.com/science/article/pii/0168192391900028>, 1991.
- Couvreux, V., Ledder, G., Manzoni, S., Way, D. A., Muller, E. B., and Russo, S. E.: Water transport through tall trees: A vertically explicit,  
440 analytical model of xylem hydraulic conductance in stems, *Plant, Cell & Environment*, 41, 1821–1839, <https://doi.org/10.1111/pce.13322>, <http://doi.wiley.com/10.1111/pce.13322>, 2018.
- Cowan, I. R.: *Transport of Water in the Soil-Plant-Atmosphere System*, Tech. Rep. 1, 1965.
- Daly, E., Porporato, A., Rodriguez-Iturbe, I., Daly, E., Porporato, A., and Rodriguez-Iturbe, I.: Coupled Dynamics of Photosynthesis, Transpiration, and Soil Water Balance. Part I: Upscaling from Hourly to Daily Level, *Journal of Hydrometeorology*, 5, 546–

- 445 558, [https://doi.org/10.1175/1525-7541\(2004\)005<0546:CDOPTA>2.0.CO;2](https://doi.org/10.1175/1525-7541(2004)005<0546:CDOPTA>2.0.CO;2), <http://journals.ametsoc.org/doi/abs/10.1175/1525-7541%282004%29005%3C0546%3ACDOPTA%3E2.0.CO%3B2>, 2004.
- Damour, G., Simonneau, T., Cochard, H., and Urban, L.: An overview of models of stomatal conductance at the leaf level, *Plant, Cell and Environment*, 33, 1419–1438, <https://doi.org/10.1111/j.1365-3040.2010.02181.x>, 2010.
- De Kauwe, M. G., Zhou, S.-X., Medlyn, B. E., Pitman, A. J., Wang, Y.-P., Duursma, R. A., and Prentice, I. C.: Do land surface models  
450 need to include differential plant species responses to drought? Examining model predictions across a mesic-xeric gradient in Europe, *Biogeosciences*, 12, 7503–7518, <https://doi.org/10.5194/bg-12-7503-2015>, [www.biogeosciences.net/12/7503/2015/](http://www.biogeosciences.net/12/7503/2015/), 2015.
- DeLucia, E. H. and Heckathorn, S. A.: The effect of soil drought on water-use efficiency in a contrasting Great Basin desert and Sierran montane species, *Plant, Cell & Environment*, 12, 935–940, <https://doi.org/10.1111/j.1365-3040.1989.tb01973.x>, 1989.
- Denmead, O. T. and Shaw, R. H.: Availability of Soil Water to Plants as Affected by Soil Moisture Content and Meteorological Con-  
455 ditions I, *Agronomy Journal*, 54, 385–390, <https://doi.org/10.2134/agronj1962.00021962005400050005x>, <http://doi.wiley.com/10.2134/agronj1962.00021962005400050005x>, 1962.
- Egea, G., Verhoef, A., and Vidale, P. L.: Towards an improved and more flexible representation of water stress in coupled photosynthesis–stomatal conductance models, *Agricultural and Forest Meteorology*, 151, 1370–1384, <https://doi.org/10.1016/J.AGRFORMET.2011.05.019>, <https://www.sciencedirect.com/science/article/pii/S0168192311001778>, 2011.
- 460 Eller, C. B., Rowland, L., Mencuccini, M., Rosas, T., Williams, K., Harper, A., Medlyn, B. E., Wagner, Y., Klein, T., Teodoro, G. S., Oliveira, R. S., Matos, I. S., Rosado, B. H. P., Fuchs, K., Wohlfahrt, G., Montagnani, L., Meir, P., Sitch, S., and Cox, P. M.: Stomatal optimization based on xylem hydraulics (SOX) improves land surface model simulation of vegetation responses to climate, *New Phytologist*, N/A, 1–16, <https://doi.org/10.1111/nph.16419>, <https://onlinelibrary.wiley.com/doi/abs/10.1111/nph.16419>, 2020.
- Farquhar, G. D., von Caemmerer, S., and Berry, J. A.: A biochemical model of photosynthetic CO<sub>2</sub> assimilation in leaves of C<sub>3</sub> species,  
465 *Planta*, <https://doi.org/10.1007/BF00386231>, 1980.
- Fatichi, S., Pappas, C., and Ivanov, V. Y.: Modeling plant-water interactions: an ecohydrological overview from the cell to the global scale, *Wiley Interdisciplinary Reviews: Water*, 3, 327–368, <https://doi.org/10.1002/wat2.1125>, <http://doi.wiley.com/10.1002/wat2.1125>, 2016.
- Feddes, R. A. and Raats, P. C.: Parameterizing the soil - water - plant root system, in: *Unsaturated-zone modeling: Progress, challenges and applications*, chap. 4, pp. 95–141, Kluwer Academic Publishers, Dordrecht, 2004.
- 470 Feddes, R. A., Kowalik, P. J., and Zaradny, H.: *Simulation of field water use and crop yield. Simulation monographs*, Halsted Press, Wageningen, 1978.
- Feng, X.: Marching in step: The importance of matching model complexity to data availability in terrestrial biosphere models, *Global Change Biology*, 26, 3190–3192, <https://doi.org/10.1111/gcb.15090>, <https://onlinelibrary.wiley.com/doi/abs/10.1111/gcb.15090>, 2020.
- Feng, X., Ackerly, D. D., Dawson, T. E., Manzoni, S., Skelton, R. P., Vico, G., and Thompson, S. E.: The ecohydrological context of drought  
475 and classification of plant responses, *Ecology Letters*, N/A, 14, <https://doi.org/10.1111/ele.13139>, 2018.
- Fisher, J. B., Lee, B., Purdy, A. J., Halverson, G. H., Dohlen, M. B., Cawse-Nicholson, K., Wang, A., Anderson, R. G., Aragon, B., Arain, M. A., Baldocchi, D. D., Baker, J. M., Barral, H., Bernacchi, C. J., Bernhofer, C., Biraud, S. C., Bohrer, G., Brunsell, N., Cappelaere, B., Castro-Contreras, S., Chun, J., Conrad, B. J., Cremonese, E., Demarty, J., Desai, A. R., De Ligne, A., Foltýnová, L., Goulden, M. L., Griffis, T. J., Grünwald, T., Johnson, M. S., Kang, M., Kelbe, D., Kowalska, N., Lim, J.-H., Mañassara, I., McCabe,  
480 M. F., Missik, J. E. C., Mohanty, B. P., Moore, C. E., Morillas, L., Morrison, R., Munger, J. W., Posse, G., Richardson, A. D., Russell, E. S., Ryu, Y., Sanchez-Azofeifa, A., Schmidt, M., Schwartz, E., Sharp, I., Šigut, L., Tang, Y., Hulley, G., Anderson, M., Hain, C., French, A., Wood, E., Hook, S., Fisher, J. B., Lee, B., Purdy, A. J., Halverson, G. H., Dohlen, M. B., and Fisher, A. L.: ECOSTRESS:

- NASA's Next Generation Mission to Measure Evapotranspiration From the International Space Station, *Water Resources Research*, 56, <https://doi.org/10.1029/2019WR026058>, <https://doi.org/>, 2020.
- 485 Fisher, R. A., Koven, C. D., Anderegg, W. R., Christoffersen, B. O., Dietze, M. C., Farrior, C. E., Holm, J. A., Hurtt, G. C., Knox, R. G., Lawrence, P. J., Lichstein, J. W., Longo, M., Matheny, A. M., Medvigy, D., Muller-Landau, H. C., Powell, T. L., Serbin, S. P., Sato, H., Shuman, J. K., Smith, B., Trugman, A. T., Viskari, T., Verbeeck, H., Weng, E., Xu, C., Xu, X., Zhang, T., and Moorcroft, P. R.: Vegetation demographics in Earth System Models: A review of progress and priorities, <https://doi.org/10.1111/gcb.13910>, <https://onlinelibrary-wiley-com.ezp1.lib.umn.edu/doi/full/10.1111/gcb.13910><https://onlinelibrary-wiley-com.ezp1.lib.umn.edu/doi/abs/10.1111/gcb.13910><https://onlinelibrary-wiley-com.ezp1.lib.umn.edu/doi/10.1111/gcb.13910>, 2018.
- 490 Franks, S. J., Weber, J. J., and Aitken, S. N.: Evolutionary and plastic responses to climate change in terrestrial plant populations, *Evolutionary Applications*, 7, 123–139, <https://doi.org/10.1111/eva.12112>, <https://onlinelibrary.wiley.com/doi/10.1111/eva.12112>, 2014.
- Gardner, W. R.: Dynamic aspects of water availability to plants, *Soil Science*, 89, 63–73, <https://doi.org/10.1097/00010694-196002000-00001>, 1960.
- 495 Goudriaan, J. and Laar, H. H. v.: *Modelling potential crop growth processes : textbook with exercises*, <https://doi.org/10.1007/978-94-011-0750-1>, 1994.
- Irvine, J., Law, B. E., Martin, J. G., and Vickers, D.: Interannual variation in soil CO<sub>2</sub> efflux and the response of root respiration to climate and canopy gas exchange in mature ponderosa pine, *Global Change Biology*, 14, 2848–2859, <https://doi.org/10.1111/j.1365-2486.2008.01682.x>, 2008.
- 500 Jarvis, P.: The interpretation of the variations in leaf water potential and stomatal conductance found in canopies in the field, Tech. rep., 1976.
- Katul, G. G., Oren, R., Manzoni, S., Higgins, C., and Parlange, M. B.: Evapotranspiration: A process driving mass transport and energy exchange in the soil-plant-atmosphere-climate system, <https://doi.org/10.1029/2011RG000366>, 2012.
- Kennedy, D., Swenson, S., Oleson, K. W., Lawrence, D. M., Fisher, R., Lola da Costa, A. C., and Gentine, P.: Implementing Plant Hydraulics in the Community Land Model, Version 5, *Journal of Advances in Modeling Earth Systems*, 11, 485–513, <https://doi.org/10.1029/2018MS001500>, <http://doi.wiley.com/10.1029/2018MS001500>, 2019.
- 505 Klein, T.: The variability of stomatal sensitivity to leaf water potential across tree species indicates a continuum between isohydric and anisohydric behaviours, *Functional Ecology*, 28, 1313–1320, <https://doi.org/10.1111/1365-2435.12289>, <http://doi.wiley.com/10.1111/1365-2435.12289>, 2014.
- Kowalczyk, E. A., Wang, Y. P., Law, R. M., Davies, H. L., McGregor, J. L., and Abramowitz, G.: The CSIRO Atmosphere Biosphere Land Exchange (CABLE) model for use in climate models and as an offline model, Tech. rep., [http://www.cmar.csiro.au/e-print/open/kowalczykea\\_2006a.pdf](http://www.cmar.csiro.au/e-print/open/kowalczykea_2006a.pdf), 2006.
- 510 Kroes, J. G., van Dam, J., Bartholomeus, R., Groenendijk, P., Heinen, M., Hendriks, R., Mulder, H., Supit, I., and van Walsum, P.: SWAP version 4: Theory description and user manual, Tech. rep., Wageningen Environmental Research, Wageningen, <https://doi.org/ISSN 1566-7197>, 2017.
- 515 Lin, C., Gentine, P., Huang, Y., Guan, K., Kimm, H., and Zhou, S.: Diel ecosystem conductance response to vapor pressure deficit is suboptimal and independent of soil moisture, *Agricultural and Forest Meteorology*, 250–251, 24–34, <https://doi.org/10.1016/J.AGRFORMET.2017.12.078>, <https://www.sciencedirect.com/science/article/pii/S0168192317304884>, 2018.
- Liu, Y., Kumar, M., Katul, G. G., Feng, X., and Konings, A. G.: Plant hydraulics accentuates the effect of atmospheric moisture stress on transpiration, *Nature Climate Change*, 10, 691–695, <https://doi.org/10.1038/s41558-020-0781-5>, <https://doi.org/10.1038/s41558-020-0781-5>, 2020.
- 520

- Medlyn, B. E., Duursma, R. A., Eamus, D., Ellsworth, D. S., Prentice, I. C., Barton, C. V. M., Crous, K. Y., De Angelis, P., FREEMAN, M., and WINGATE, L.: Reconciling the optimal and empirical approaches to modelling stomatal conductance, *Global Change Biology*, 17, 2134–2144, <https://doi.org/10.1111/j.1365-2486.2010.02375.x>, <http://doi.wiley.com/10.1111/j.1365-2486.2010.02375.x>, 2011.
- Medlyn, B. E., De Kauwe, M. G., Zaehle, S., Walker, A. P., Duursma, R. A., Luus, K., Mishurov, M., Pak, B., Smith, B., Wang, Y.-P., Yang, X., Crous, K. Y., Drake, J. E., Gimeno, T. E., Macdonald, C. A., Norby, R. J., Power, S. A., Tjoelker, M. G., and Ellsworth, D. S.: Using models to guide field experiments: a priori predictions for the CO<sub>2</sub> response of a nutrient- and water-limited native Eucalypt woodland, *Global Change Biology*, 22, 2834–2851, <https://doi.org/10.1111/gcb.13268>, <http://doi.wiley.com/10.1111/gcb.13268>, 2016.
- Medvigy, D., Wofsy, S. C., Munger, J. W., Hollinger, D. Y., and Moorcroft, P. R.: Mechanistic scaling of ecosystem function and dynamics in space and time: Ecosystem Demography model version 2, *Journal of Geophysical Research: Biogeosciences*, 114, G01002, <https://doi.org/10.1029/2008JG000812>, <http://doi.wiley.com/10.1029/2008JG000812>, 2009.
- Mencuccini, M., Manzoni, S., and Christoffersen, B. O.: Modelling water fluxes in plants: from tissues to biosphere, *New Phytologist*, <https://doi.org/10.1111/nph.15681>, 2019.
- Novick, K. A., Ficklin, D. L., Stoy, P. C., Williams, C. A., Bohrer, G., Oishi, A. C., Papuga, S. A., Blanken, P. D., Noormets, A., Sulman, B. N., Scott, R. L., Wang, L., and Phillips, R. P.: The increasing importance of atmospheric demand for ecosystem water and carbon fluxes, *Nature Climate Change*, 6, 1023–1027, <https://doi.org/10.1038/nclimate3114>, 2016.
- Oleson, K. W., Lead, D. M. L., Bonan, G. B., Drewniak, B., Huang, M., Koven, C. D., Levis, S., Li, F., Riley, W. J., Subin, Z. M., Swenson, S. C., Thornton, P. E., Bozbiyik, A., Fisher, R., Heald, C. L., Kluzek, E., Lamarque, J.-F., Lawrence, P. J., Leung, L. R., Lipscomb, W., Muszala, S., Ricciuto, D. M., Sacks, W., Sun, Y., Tang, J., and Yang, Z.-L.: Technical Description of the version 5.0 of the Community Land Model (CLM), Tech. rep., [http://www.cesm.ucar.edu/models/cesm2/land/CLM50\\_Tech\\_Note.pdf](http://www.cesm.ucar.edu/models/cesm2/land/CLM50_Tech_Note.pdf)<http://library.ucar.edu/research/publish-technote>, 2018.
- Pammenter, N. W. and Willigen, C. V.: A mathematical and statistical analysis of the curves illustrating vulnerability of xylem to cavitation, in: *Tree Physiology*, <https://doi.org/10.1093/treephys/18.8-9.589>, 1998.
- Paschalis, A., Fatichi, S., Zscheischler, J., Ciais, P., Bahn, M., Boysen, L., Chang, J., De Kauwe, M., Estiarte, M., Goll, D., Hanson, P. J., Harper, A. B., Hou, E., Kigel, J., Knapp, A. K., Larsen, K. S., Li, W., Lienert, S., Luo, Y., Meir, P., Nabel, J. E., Ogaya, R., Parolari, A. J., Peng, C., Peñuelas, J., Pongratz, J., Rambal, S., Schmidt, I. K., Shi, H., Sternberg, M., Tian, H., Tschumi, E., Ukkola, A., Vicca, S., Viovy, N., Wang, Y. P., Wang, Z., Williams, K., Wu, D., and Zhu, Q.: Rainfall manipulation experiments as simulated by terrestrial biosphere models: Where do we stand?, *Global Change Biology*, 26, 3336–3355, <https://doi.org/10.1111/gcb.15024>, <https://onlinelibrary-wiley-com.ezp1.lib.umn.edu/doi/full/10.1111/gcb.15024><https://onlinelibrary-wiley-com.ezp1.lib.umn.edu/doi/abs/10.1111/gcb.15024><https://onlinelibrary-wiley-com.ezp1.lib.umn.edu/doi/10.1111/gcb.15024>, 2020.
- Powell, T. L., Galbraith, D. R., Christoffersen, B. O., Harper, A., Imbuzeiro, H. M., Rowland, L., Almeida, S., Brando, P. M., da Costa, A. C. L., Costa, M. H., Levine, N. M., Malhi, Y., Saleska, S. R., Sotta, E., Williams, M., Meir, P., and Moorcroft, P. R.: Confronting model predictions of carbon fluxes with measurements of Amazon forests subjected to experimental drought, *New Phytologist*, 200, 350–365, <https://doi.org/10.1111/nph.12390>, 2013.
- Prentice, I. C., Liang, X., Medlyn, B. E., and Wang, Y.-P.: Reliable, robust and realistic: the three R's of next-generation land-surface modelling, *Atmospheric Chemistry and Physics*, 15, 5987–6005, <https://doi.org/10.5194/acp-15-5987-2015>, <https://www.atmos-chem-phys.net/15/5987/2015/>, 2015.

- Razavi, S., Sheikholeslami, R., Gupta, H. V., and Haghnegahdar, A.: VARS-TOOL: A toolbox for comprehensive, efficient, and robust sensitivity and uncertainty analysis, *Environmental Modelling and Software*, 112, 95–107, <https://doi.org/10.1016/j.envsoft.2018.10.005>, 2019.
- 560 Restrepo-Coupe, N., Levine, N. M., Christoffersen, B. O., Albert, L. P., Wu, J., Costa, M. H., Galbraith, D., Imbuzeiro, H., Martins, G., da Araujo, A. C., Malhi, Y. S., Zeng, X., Moorcroft, P., and Saleska, S. R.: Do dynamic global vegetation models capture the seasonality of carbon fluxes in the Amazon basin? A data-model intercomparison, *Global Change Biology*, 23, 191–208, <https://doi.org/10.1111/gcb.13442>, <http://doi.wiley.com/10.1111/gcb.13442>, 2017.
- Rogers, A., Medlyn, B. E., Dukes, J. S., Bonan, G., von Caemmerer, S., Dietze, M. C., Kattge, J., Leakey, A. D. B., Mercado, L. M., Ni-  
 565 inemets, , Prentice, I. C., Serbin, S. P., Sitch, S., Way, D. A., and Zaehle, S.: A roadmap for improving the representation of photosynthesis in Earth system models, *New Phytologist*, 213, 22–42, <https://doi.org/10.1111/nph.14283>, <http://doi.wiley.com/10.1111/nph.14283>, 2017.
- Sabot, M. E. B., De Kauwe, M. G., Pitman, A. J., Medlyn, B. E., Verhoef, A., Ukkola, A. M., and Abramowitz, G.: Plant profit maximization improves predictions of European forest responses to drought, *New Phytologist*, N/A, 1–18, <https://doi.org/10.1111/nph.16376>, <https://onlinelibrary.wiley.com/doi/abs/10.1111/nph.16376>, 2020.
- 570 Schwarz, P. A., Law, B. E., Williams, M., Irvine, J., Kurpius, M., and Moore, D.: Climatic versus biotic constraints on carbon and water fluxes in seasonally drought-affected ponderosa pine ecosystems, *Global Biogeochemical Cycles*, 18, 1–17, <https://doi.org/10.1029/2004GB002234>, 2004.
- Sitch, S., Huntingford, C., Gedney, N., Levy, P. E., Lomas, M., Piao, S. L., Betts, R., Ciais, P., Cox, P. M., Friedlingstein, P., Jones, C. D., Prentice, I. C., and Woodward, F. I.: Evaluation of the terrestrial carbon cycle, future plant geography and climate-carbon cycle feed-  
 575 backs using five Dynamic Global Vegetation Models (DGVMs), *Global Change Biology*, 14, 2015–2039, <https://doi.org/10.1111/j.1365-2486.2008.01626.x>, <http://doi.wiley.com/10.1111/j.1365-2486.2008.01626.x>, 2008.
- Sperry, J. S. and Love, D. M.: What plant hydraulics can tell us about responses to climate-change droughts, *New Phytologist*, 207, 14–27, <https://doi.org/10.1111/nph.13354>, <http://doi.wiley.com/10.1111/nph.13354>, 2015.
- Sperry, J. S., Adler, F. R., Campbell, G. S., and Comstock, J. P.: Limitation of plant water use by rhizosphere and xylem conductance: Results  
 580 from a model, *Plant, Cell and Environment*, 21, 347–359, <https://doi.org/10.1046/j.1365-3040.1998.00287.x>, 1998.
- Trugman, A. T., Medvigy, D., Mankin, J. S., and Anderegg, W. R.: Soil Moisture Stress as a Major Driver of Carbon Cycle Uncertainty, *Geophysical Research Letters*, 45, 6495–6503, <https://doi.org/10.1029/2018GL078131>, 2018.
- Ukkola, A. M., De Kauwe, M. G., Pitman, A. J., Best, M. J., Abramowitz, G., Haverd, V., Decker, M., and Houghton, N.: Land surface models systematically overestimate the intensity, duration and magnitude of seasonal-scale evaporative droughts, *Environmental Research Letters*,  
 585 11, 104 012, <https://doi.org/10.1088/1748-9326/11/10/104012>, <https://iopscience.iop.org/article/10.1088/1748-9326/11/10/104012https://iopscience.iop.org/article/10.1088/1748-9326/11/10/104012/meta>, 2016.
- Ukkola, A. M., Houghton, N., De Kauwe, M. G., Abramowitz, G., and Pitman, A. J.: FluxnetLSM R package (v1.0): a community tool for processing FLUXNET data for use in land surface modelling, *Geosci. Model Dev*, 10, 3379–3390, <https://doi.org/10.5194/gmd-10-3379-2017>, <https://doi.org/10.5194/gmd-10-3379-2017>, 2017.
- 590 Verhoef, A. and Egea, G.: Modeling plant transpiration under limited soil water: Comparison of different plant and soil hydraulic parameterizations and preliminary implications for their use in land surface models, *Agricultural and Forest Meteorology*, 191, 22–32, <https://doi.org/10.1016/J.AGRFORMET.2014.02.009>, <https://www.sciencedirect.com/science/article/pii/S0168192314000483>, 2014.
- Williams, M., Law, B. E., Anthoni, P. M., and Unsworth, M. H.: Use of a simulation model and ecosystem flux data to examine carbon-water interactions in ponderosa pine, *Tree Physiology*, 21, 287–298, <https://doi.org/10.1093/treephys/21.5.287>, 2001.

- 595 Wolf, A., Anderegg, W. R. L., and Pacala, S. W.: Optimal stomatal behavior with competition for water and risk of hydraulic impairment., *Proceedings of the National Academy of Sciences of the United States of America*, 113, E7222–E7230, <https://doi.org/10.1073/pnas.1615144113>, <http://www.ncbi.nlm.nih.gov/pubmed/27799540>, 2016.
- Xu, X., Medvigy, D., Powers, J. S., Becknell, J. M., and Guan, K.: Diversity in plant hydraulic traits explains seasonal and inter-annual variations of vegetation dynamics in seasonally dry tropical forests, *New Phytologist*, 212, 80–95, <https://doi.org/10.1111/nph.14009>,  
600 <http://doi.wiley.com/10.1111/nph.14009>, 2016.
- Yang, S. J. and de Jong, E.: Effect of Aerial Environment and Soil Water Potential on the Transpiration and Energy Status of Water in Wheat Plants I, *Agronomy Journal*, 64, 574–578, <https://doi.org/10.2134/agronj1972.00021962006400050006x>, <http://doi.wiley.com/10.2134/agronj1972.00021962006400050006x>, 1972.
- Zhang, Q., Manzoni, S., Katul, G., Porporato, A., and Yang, D.: The hysteretic evapotranspiration-Vapor pressure deficit relation,  
605 *Journal of Geophysical Research: Biogeosciences*, 119, 125–140, <https://doi.org/10.1002/2013JG002484>, <http://doi.wiley.com/10.1002/2013JG002484>, 2014.
- Zhou, S., Duursma, R. A., Medlyn, B. E., Kelly, J. W., and Prentice, I. C.: How should we model plant responses to drought? An analysis of stomatal and non-stomatal responses to water stress, *Agricultural and Forest Meteorology*, 182–183, 204–214, <https://doi.org/10.1016/J.AGRFORMET.2013.05.009>, <https://www.sciencedirect.com/science/article/pii/S0168192313001263>, 2013.